

A general model of how fire emissions and chemistry produce African/oceanic plumes (O₃, CO, PAN, smoke) in TRACE A

Robert B. Chatfield,¹ John A. Vastano,² H.B. Singh,¹ and G. Sachse³

Abstract. A full-chemistry simulation of the Great African Plume gives one example of a broad conceptual model of the intercontinental pollution of the tropical middle troposphere by lofted biomass burning plumes. This two-dimensional idealization “calibrated” by carbon monoxide distributions links conventional estimates of burning emissions to oceanic concentrations of pollutants. This paper makes use of GRACES, a modular photochemical simulation system, in two forms. The results of the chemically intensive two-dimensional form, using idealized winds, mixing, deposition, and rainout, match the general concentration patterns of a three-dimensional GRACES model study of CO during the TRACE A/SAFARI period of October 1992 (reported separately). The study highlights the importance of simulating the vertical and diurnal variation of the planetary boundary layer and cloud activity. These correlate temporally with the intensity of tropical agricultural burning. We emphasize one situation, the drift northward and eastward of pollution into the interoceanic convergence region, where it rises by small-scale motions and rides out westward in the lower midtroposphere (<5 km). These effects help set in place large strata of enhanced CO, ozone, and other pollution over the equatorial Atlantic Ocean. Overall, our comparisons of simulations with the TRACE A data on the cycling of CO, NO_x, and O₃ in the tropical atmosphere suggest substantial agreement of current emission estimates and atmospheric concentrations. In certain regions, ozone is simulated slightly below observed levels. The striking major disagreements are in NO_y (total reactive nitrogen) and HNO₃, which are intimately related to CO and O₃; this suggests that current theory omits at least one fundamental process.

Introduction

A great change in scientific outlook accompanied the discovery of an accumulation of ozone in the troposphere above the equatorial Atlantic and its adjacent continents, South America and Africa [Crutzen *et al.*, 1985; Logan and Kirchoff, 1986; Marengo *et al.*, 1990; Fishman *et al.*, 1991]. Previous description had been of the spread of pollution from midlatitude cities and industries, especially in the northern midlatitudes [Seiler, 1974]. From the beginning the fragmentary satellite estimates of midtropospheric carbon monoxide [Connors *et al.*, 1991] and the seasonality of the ozone maximum [Logan and Kirchoff, 1986] suggested that some sort of anthropogenic pollution might play a role. This CO pollution was not from midlatitude industry, and the ozone was not industrial pollution augmented by midlatitude stratospheric intrusions, as two-dimensional models of the troposphere had suggested, and as the GAMETAG measurements, meridional transects of ozone and carbon monoxide [Routhier *et al.*, 1980; Heidt *et al.*, 1980] had seemingly confirmed. Rather, the implicated pollution source was the large-scale burning of biomass, burning associated with agricultural crop residues,

pasture and grassland material, as well as rain forest clearing [Crutzen *et al.*, 1985; Chatfield and Delany, 1990]. This pattern seemed to reveal large-scale anthropogenic modification of tropospheric ozone more clearly than in the highly industrialized northern latitudes.

However, a puzzling aspect of the tropospheric ozone residual maps provided by Fishman *et al.* [1991] was the high values, often maxima, of ozone column over the central equatorial Atlantic, 3000 km from the supposed source regions in Africa and South America. In the northern midlatitudes, carbon monoxide and ozone pollution were very concentrated in thousand-kilometer regions around industrial-urban sources. Chatfield and Delany [1990] outlined one process that could transport ozone from high-altitude cumulonimbus outflow from South America, and Scala *et al.* [1990] and Pickering *et al.* [this issue (a)] (and references) have illustrated several specific examples of the process. While this process seems to explain a significant portion of the ozone in the mid-Atlantic, most of the ozone appears to arrive from Africa. As Thompson *et al.* [this issue] point out, the high mixing ratios of upper tropospheric ozone over Ascension Island, attributable to deep convective processes over Southern America, contribute only 20–30% of the observed high-ozone excess column abundance over clean tropospheric expected values. Other ozone sources are required.

Besides illustrating deep cloud convection effects, this paper illustrates another mechanism by which midtropospheric ozone can arise from the dry, elevated grasslands typical of South America and especially southern Africa. It emphasizes dry and nonpenetrative convection. There are two additional factors: (a) the coincidence of biomass burning, boundary layer mixing, and cloud convection in the afternoon may be important and also (b)

¹NASA Ames Research Center, Moffett Field, California.

²San Jose State University, San Jose, California.

³NASA Langley Research Center, Hampton, Virginia.

the role of localized organized convergence/patterns in the lower troposphere, e.g., an interocean front, to the north and east of the emissions. These aspects of the convective process are repeatedly suggested by our simulations, but evaluation will require further studies. These important effects support the importance of the "mix and cook" situations described by *Chatfield and Delany* [1990], in which situations of biomass burning followed within hours by deep cumulus convection was found to be particularly effective in elevating the tropospheric ozone column.

Two large field experiments, Tropical Atmospheric Chemistry Experiment Atlantic (TRACE A) and Southern African Fire Atmospheric Research Initiative (SAFARI), were mounted in September and October 1992, to sample the pollutant sources and mid-oceanic accumulation [*Andreae et al.*, 1994; *Bachmeier and Fuelberg*, this issue; *Fishman et al.* [this issue], *Thompson et al.*, this issue]. The work reported here is intended to summarize one important process at work during that sampling period and to make some general comparisons to the TRACE A data.

Outline of the Paper

Our transport-chemistry model, GRACES (Global-Regional Atmospheric Chemistry Event Simulator), is used in two ways. In one mode it uses highly realistic three-dimensional winds and cloud transports to describe the motion of an inert tracer, one that behaves like carbon monoxide. A striking and repeated feature of this simulation seems to deserve more detailed chemical simulation. After an introductory description of this simulation we describe some preliminary results which motivated the main chemistry simulation that constitute this paper. Further three-dimensional analysis will come in a future paper, but this striking feature of the three-dimensional simulations causes us to seek to formulate a simple but general model of biomass plumes.

Thus motivated, we return to model formulation, and propose a two-dimensional Great African Plume model that follows one main pathway of the plume that has very visible effects in Atlantic Ocean. This model also attempts to have just enough description of transport to rationalize the concentrations seen in the atmosphere with the emission fluxes of pollutants and other trace species. Yet, it retains the simplicity to provide a reasonably simple conceptual framework for comparing the roles of important processes. In some important ways, it overcomes some limitations of the trajectory models which have also been applied to explain the TRACE A observations. In a few days the atmosphere significantly acts both to accumulate pollution like CO and to disperse it horizontally and to vent it vertically. Since it is difficult to simulate these processes in trajectory models, their results are more limited in addressing emission/concentration budget questions and dispersion. The trajectory models, of course, being conceptually simpler, are even more rapidly and broadly deployable and give some three-dimensional information consistent with resolvable analyzed wind fields [*Thompson et al.*, this issue; *Fuelberg et al.*, this issue; *Pickering et al.*, this issue(b)]. We expect that our proposed model has complementary capabilities and limitations.

Following the description of the idealization there is a section on methods for emission and chemistry. The two-dimensional results are analyzed, first to describe qualitatively the very different biomass burning plumes that different species trace out and then to make initial comparisons to a small set of the TRACE A data showing general agreement. However, nitric acid in the continental plume and ozone production in the far-downwind ocean plume show disagreements with observations; these require

explanations that are beyond our paper. This connects our simulation to the local-photochemical model work also performed for TRACE A [*Jacob et al.*, this issue; *Thompson et al.*, this issue; *Pickering et al.*, this issue].

Motivation

Three-Dimensional Simulation of TRACE A Burning Emissions

How do ozone and CO accumulate so in the central Atlantic? Weather patterns vary sufficiently in the tropics that we attempt to describe a typical main route, with typical transit times, rather than one constituted on mean winds. Our current purpose is to provide an appropriate setting for a specialized two-dimensional model; that is, a generalized picture of emission, vertical mixing, and transport in a general downwind direction, and one typical pattern will serve. We draw that pattern from a three-dimensional simulation of a carbon monoxide-like tracer using reconstructed meteorological winds and patterns of dry (boundary layer) and moist convection.

Methods for three-dimensional simulations

MM5 runs. Plates 1a and 1b give a multilevel view of an important October flow pattern centered on southern and central Africa, taken from a run of the MM5 mesoscale-synoptic model [*Grell et al.*, 1994, and references]. This figure portrays the weather-simulation and forecasting model, MM5, run in an assimilation mode, for 1300 UT on October 2, 1992. The model nudges the solutions toward the observed meteorology as recorded in the analyses of the European Centre for Medium-Range Weather Forecasting (ECMWF) [*Grell et al.*, 1994]. Special analyses for the TOGA (Tropical Ocean Global Atmosphere) period were available for 1992 with better-than-normal observational support. A standard Blackadar technique described in the MM5 documentation was used to simulate the planetary boundary layer. Plate 1c shows the diagnosed boundary layer height, above the surface, for that time. The Grell scheme [*Grell*, 1993; *Grell et al.*, 1994, and references] developed for MM5 (version 1) was used to simulate convection. Plates 1d and 1e show the simulated cloud updraft top in kilometers and the cloud base updraft mass flux for the same time. Clearly, the cloud top diagnostic should be interpreted judiciously outside the regions of larger mass flux. No separate, special low-cloud parameterization was employed; the difficulty of detailed low-cloud simulation justifies more specialized work. The convective mass flux information as well as a boundary layer height and convective velocity-scale information were saved for off-line use. All the wind, density, and convective information were transferred into our GRACES model, run in a three-dimensional mode.

GRACES is our Global-Regional Atmospheric Chemistry Event Simulator, to be more fully described by R. B. Chatfield et al. (manuscript in preparation, 1996) (hereinafter referred to as C). Briefly, it is modularly constructed and runs in a generalized map-projection coordinate system deriving from the description of *Toon et al.* [1988]. It employs the exponential-fit system of that paper for vertical transport, but an *S*-tuned nonoscillatory version of the *Smolarkiewicz* [1984] horizontal transport scheme. The chemistry is described by a reaction table, and the photochemistry is driven by delta-Eddington integrated intensities that are integrated with the absorptions and quantum yields of *Madronich and Calvert* [1990]. The chemistry is integrated using the DASSL algorithm employing backward difference formulae [*Brenan et*

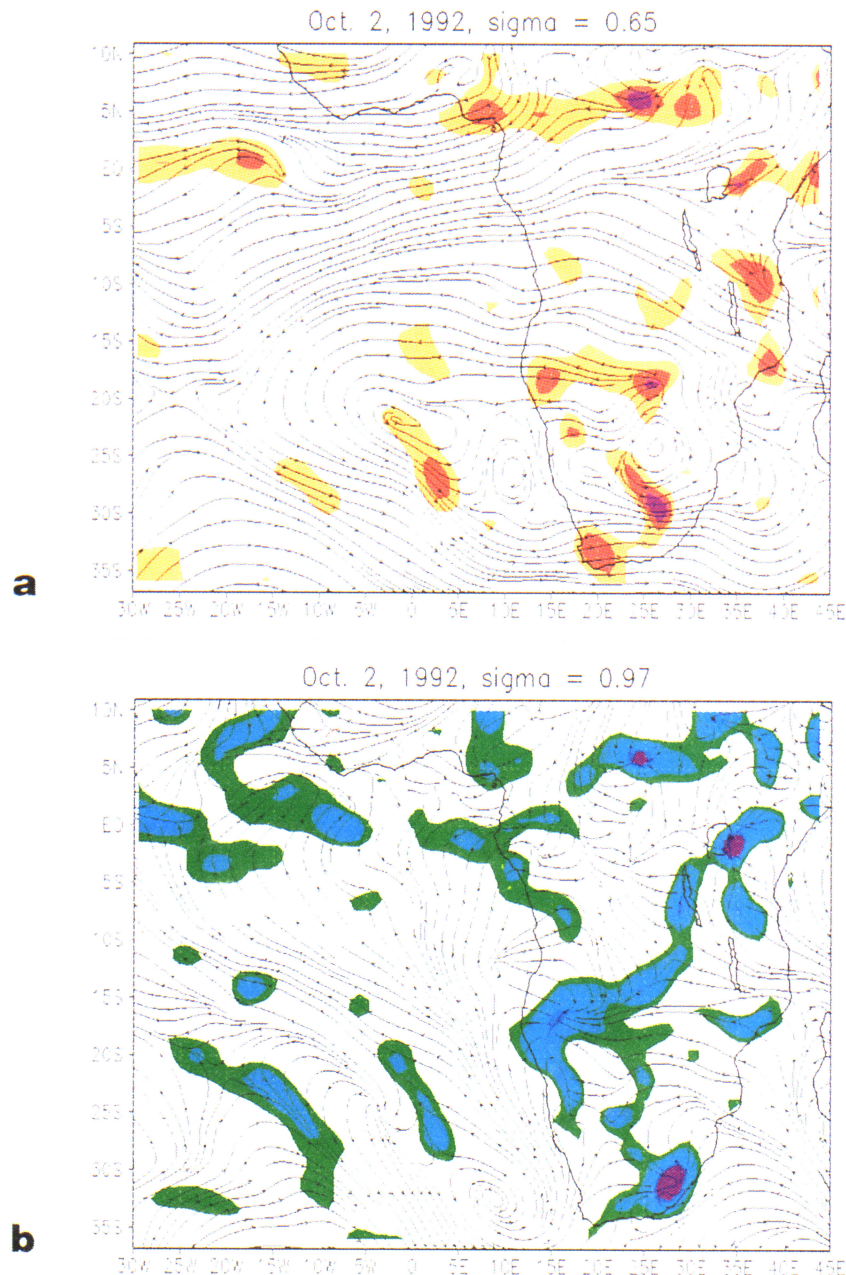


Plate 1.(a) Flow fields reconstructed by the MM5 meteorological model assimilating ECMWF winds, for October 2, 1992, 1300 UT. Wind streamlines along the $\sigma = 0.67$ surface (about 3500 m over local topography), showing easterly outflow of air from the eastern central African coast from 17°S to 5°N; this air rides up over the westerly monsoon layer beneath. In this situation, air to the south of 32°S exits South Africa into Indian Ocean westerlies, while air between approximately 17°S and 32°S recirculates over South Africa. Contours of wind divergence of 1, 1.5 and $2 \times 10^{-5} \text{ s}^{-1}$ are shown. (b) Streamlines indicating airflow at $\sigma = 0.97$ surface (about 300 m over local topography), showing inflow regions bringing clean air toward central southern Africa from 30°S to 10°S along the eastern coast of southern Africa, and also a monsoon inflow from 5°S to approximately the equator. Contours of horizontal wind convergence of 1, 1.5 and $2 \times 10^{-5} \text{ s}^{-1}$ are also shown. (c) Planetary boundary layer height reported from the MM5 model for 1300 UT; note the very deep 3- to 4.5-km convective boundary layer heights near the Kalahari (20° W, 20-27° S). (d) Cloud tops reported by the model. These are truly significant only where cloud activity is strong. (e) Cloud base mass flux in $\text{g m}^{-2} \text{ s}^{-1}$ for the updraft column of the Grell cumulus parameterization (see text). Both cloud mass fluxes and cloud tops highlight convergence zones with a complex relation to the boundary layer convergence patterns of Plates 1a and 1b.

al., 1989). It is controlled by self-documenting ASCII files, or NetCDF files [R*ew*, 1990], for higher-dimension inputs. The dimensionality of the model is controlled by program switches. The model can accept either three-dimensional, time-varying wind

fields or more idealized, time-static wind field descriptions. Planetary boundary layer mixing is controlled by setting vertical diffusivity profiles and magnitudes on the basis of model weather data (for three-dimensional model integrations) or surface heat

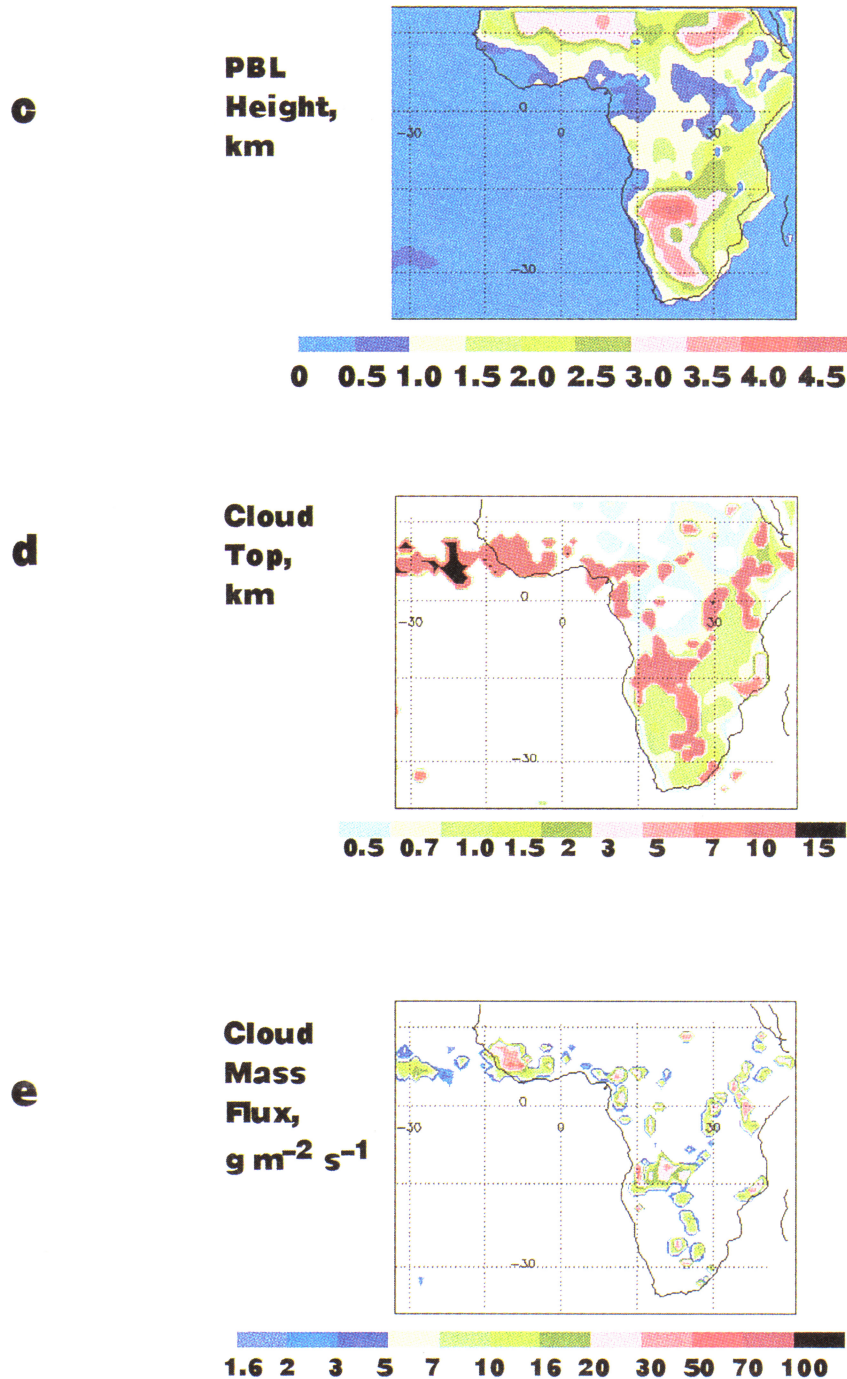


Plate 1. (continued)

fluxes and boundary layer heights (for idealized simulations), using textbook formulae with K_z values maximizing at levels at about two thirds of the mixed layer height [Seinfeld, 1986, p. 594]. Model output of species concentrations and certain diagnostic data on chemical and transport fluxes is recorded in self-documenting NetCDF files.

Following input of the MM5 data, GRACES was then used to integrate the emission fields of CO deduced from W.M. Hao's climatological database of biomass burning at 5° resolution. [Hao and Liu, 1994]. We used only the savanna-type burning, not forest burning, since we intended to highlight the role of transport from

the largest burning regions of the more southern portions of the African continent. The forest-burning component is also smaller. All of the MM5, GRACES, and emission-estimation work is described more extensively in our forthcoming paper on three-dimensional modeling (C); this paper reports on and uses only the most striking and repeated pattern. Certainly, just because our model is nudged to come very close to the ECMWF analyses, there may still be differences of analysis for the exact weather obtaining over the central Atlantic [Pickering *et al.*, this issue (a)], especially when sensitive calculations like trajectories are attempted. While the pattern might be glimpsed in Plate 1, in

general, the winds and weather of Africa are sufficiently variable that it takes a tracer integration through time to see overall transport patterns and timescales; we suggest that these features, integrated on a broad geographic scale, are much more robust than individual analyses.

Three-dimensional results. Plate 2 shows just such a repeated pattern that we find in the three-dimensional work: the transport of great plumes of CO off the west coast from equatorial Africa, westward, often southwestward toward the equatorial Atlantic region near the Greenwich meridian and 15°S, i.e., the region of persistent ozone accumulation [Fishman *et al.*, 1991]. The plumes vary but typically range from 5° to 15° latitude wide, perhaps twice as long, and extend from 1 km to 6 km in altitude. The plumes become thinned by shear into filamentous plumes as they travel westward across the Atlantic. The feature over southern and central Africa and the adjacent ocean, in several variations, is what we call the Great African Plume. It is a broader expression of the trajectory results reported by Thompson *et al.* [this issue]. We find this transport pattern from the complete simulation sufficiently strong and repeated to motivate our discussion of a full-chemistry two-dimensional simulation. Transport processes from South America tend to follow the cloud-pumping mechanism suggested for that region by Chatfield and Delany [1990] and emphasized for the TRACE A period by Pickering *et al.* [this issue]. Repeated patterns of influence originating in the cerrado and moving out of the southern Brazilian moist regions do form plumes much thinner than the African plumes and which move faster but have less effect on the equatorial Atlantic.

Return again to Plate 1 for one glimpse at the origin of the Great African Plume. This one day was chosen to represent one of several periods in which pollutant material moved offshore to the west. Plate 1a shows the airflow about 300 m above the local surface in MM5 model ($\sigma = 0.97$). At this level, air flows in from a variety of directions toward a convergence line stretching between 18°S and 10°S; most of the flow is from the east and south. Plate 1b shows the flow at $\sigma = 0.67$, at about 3.4 km above

the local terrain. While we have not completed analysis, this convergence region (and those to the northwest) appears to be a manifestation of the intertropical front. A divergence region sits above the convergence region of Plate 1a; it fades out within a kilometer above this level. At this σ level, there is a broad coordinated flow offshore and to the east, with a small portion of the air turning south; analyses we do not exhibit show that this feature is prominent in the atmospheric flow fields from $\sigma = 0.8$ (~2 km) to $\sigma = 0.4$ (~7 km), retreating to the north and increasingly recirculating up to $\sigma = 0.2$ (~12 km). Probably as significant as the organized flow is the turbulent transport in the strongly convective boundary layers prevalent in daytime. Plate 1c shows the depth of the boundary layer diagnosed for 1300 UT by MM5: the boundary layer top reaches 2–4.5 km over the surface. Maximum values are shown over the driest regions of southern Africa, like the Kalahari Desert. Plate 1d shows convective cloud tops described by the Grell parameterization. These should be most directly relatable to observables like effective cloud top temperatures where the mass flux of Plate 1e is large. Nevertheless, some degree of low cloudiness is suggested throughout the convergence region.

Did these models simulate African weather well enough during this period? Figure 1 shows an analysis for October 1, 1992, of remote sensing advanced very high resolution radiometer (AVHRR) data, part of the TRACE A data archive [Justice *et al.*, this issue; Kendall *et al.*, 1995]. The infrared analysis shows several things of interest. First, cloud cover was very similar to the cloud cover that we portray for the weather of October 2 (Plate 1). (October 2 has a clearer portrayal of African outflow; October 1 shows convergence activity better). Indeed, our meteorological analysis is very similar for central and southern Africa on these days. A region of >25% cloudiness extends eastward from the Atlantic at 10°–15°S and joins a region of cloudiness extending up from South Africa, and heads in a northeasterly direction toward the equator, very much as in Plate 1. Uninterpreted AVHRR data for the October 2 concurs with this picture. Second, there are

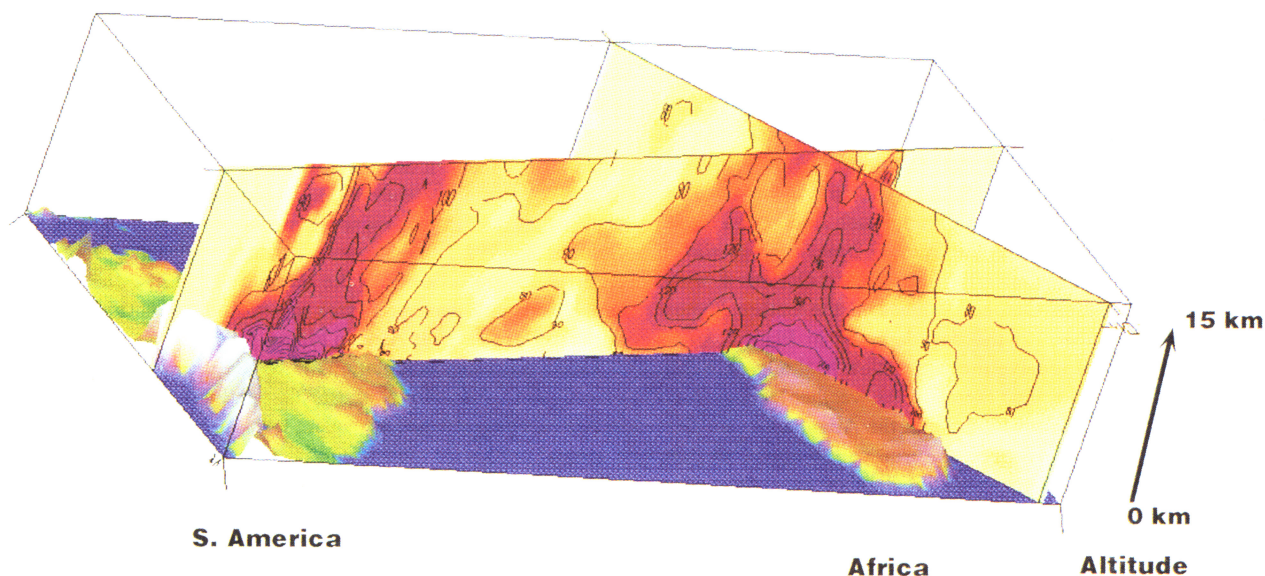


Plate 2. Simulation of the outflow of a carbon monoxide-like tracer from southern and equatorial Africa in the Great African Plume, as reconstructed for October 10, 1992; vertical cuts through the model output layer extend in an altitude scale from 0 to 15 km. Contours of carbon monoxide in parts per billion by volume. Winds and cloud transport taken from an assimilation using MM5. Note that outflow from Africa is primarily at midtropospheric altitudes, while outflow from South America is mediated by deep-cloud convective transport to the upper troposphere.

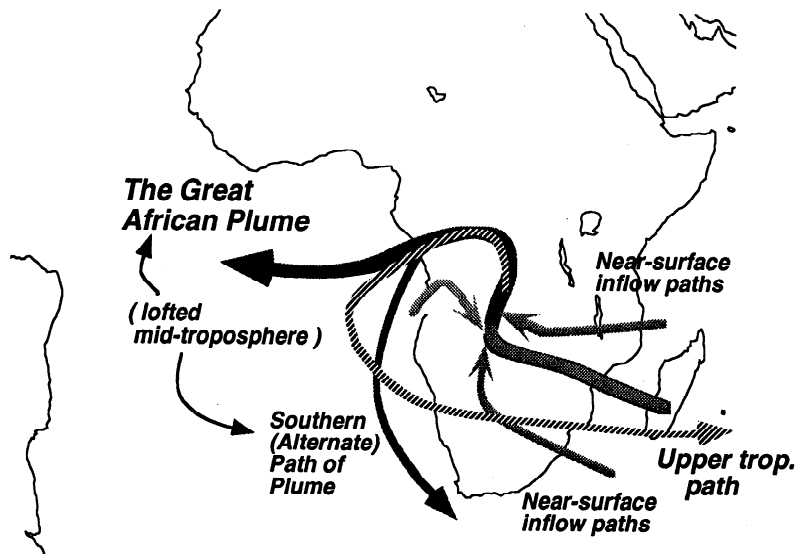


Figure 1. Path followed by air at all levels in our idealized two-dimensional chemistry model. In fact, the two-dimensional model has to represent a wider, 500- to 1500-km region in which eddies of various sizes may stir the emissions. The paths also diverge at the entry and exit regions. Individual weather maps and our tracer study suggest that there may be a variety of entry points for airflow across Africa, and also that once material moves offshore, it may wander into one or two major plumes. Some preferred directions are indicated, to the west, and down the African coast just off the western shore.

important fires on this day along the east coast of Africa. The satellite analyses cited suggest that these regions of clustered big fire counts vary considerably from day to day. However, the whole of Africa from 7°S to 23°S had the greatest fire pixel counts in September and October 1992, with a scattering of important fire pixel concentrations mostly down the southeast coast of Africa to 33°S [Kendall *et al.*, 1995].

Our broad interpretation of the meteorology of October 2, 1992, is that pollution gathers over southern Africa, is lofted by daytime turbulence and some organized vertical motion at the interocean front (intertropical front), and then flows northward and then westward out over the Atlantic Ocean; it flows over a lower moist “monsoon” inflow before it reaches the Atlantic coast. Even our preliminary analysis shows that the exact location and directionality of these features varies considerably in time. However, it is this day that appears to help spawn the clear manifestation of the Great African Plume such as is seen in Plate 2. Analysis so far suggests that the October 2 meteorology shown leads to an outbreak of the easterly plume around October 4, while similar meteorology on October 9 leads to the outbreak most visible around October 12, the day depicted in Plate 2. (This pattern of events will receive more attention in the work of C). Figure 1 provides a schematic sketch of the weather leading to the outbreak of a Great African Plume into the Atlantic Ocean. That figure can only begin to suggest the true variability of weather patterns and the degree of convoluted recirculation possible in the South Africa area.

Other work. Other work emphasizes other aspects of transport. The origin of midtropospheric air, bearing a great fraction of additional pollutant ozone in the midAtlantic, is clearly from Africa [Thompson *et al.*, this issue; Fishman *et al.*, this issue]. The origin of the air leaving the western Africa coast is less clear in other work, but a meandering drift northward from the predominant savanna-type burning regions is clear; perhaps 3-5 days are required for this drift [Pickering *et al.*, this issue; Singh *et*

al., this issue; Thompson *et al.*, this issue]. Garstang *et al.* [this issue] and Tyson *et al.* [1995] have described a variety of significant flow patterns and features over southern Africa; the major pattern of Figure 1 resembles just one. The analyses of these papers tends to center on the SAFARI region of South Africa and Zimbabwe; they stress the motion southward from the tip of South Africa (just visible south of 30°S for the meteorology of Plate 1b and also a pattern in which air curls around the Atlantic coast of South Africa to the southern Indian Ocean). A path much like this is labeled “alternate path” in Figure 1, though the circulation is often more circular and does not extend so far north. No doubt these pathways are important, and particularly for emissions originating from 22°S or farther south.

Our view is that the meteorology of Plate 1 is not persistent, but when it does recur, it does produce effects in the slow-moving air of the equatorial Atlantic that are persistent. Furthermore, we expect that it is in just those periods when flow conditions like October 2, 1992 (Plate 1) occur, then we witness the origin of significant pollution of the equatorial mid-Atlantic. Our simulations pull these processes together to reveal the source and chemistry of the Great African Plume.

Other trajectory calculations have been made by a variety of investigators. Fuelberg *et al.* [this issue], for the TRACE A period in Africa, suggest a not infrequent northward drift of polluted air, a general northward motion amid considerable recirculation in the lower troposphere of southern Africa, as suggested also in the bottom section of Plate 1. Zenker *et al.* [1995] indicate more flow from the east coast of Africa, also seen in Figure 1. Krishnamurti *et al.* [this issue] have also emphasized transport from the upper troposphere over the burning areas of tropical continents toward the accumulation region. Other backward trajectory calculations made from 1- to 4-km-high endpoints in the central Atlantic frequently trace back to equatorial Africa, as is suggested by the $\sigma = 0.69$ (~ 3.4 km above topography) analysis in the upper portion of Plate 1. However, all these trajectory analyses lack a

description of the vertical mixing process; moreover, they lack appropriate emission, ventilation, and deposition processes for the pollutants that allow budgeting and closure of chemical cycles.

A Two-Dimensional Idealization of the Great African Plume

The idealized trajectory that we will use for a chemistry simulation draws from the three-dimensional simulation discussed above and is shown in Plate 3. Note the similarity of the ground traces in Figure 1 to portions of the two vertical walls shown in Plate 2. In the idealization, air follows a path as a vertical curtain following some generalized effective winds: air at all levels must be idealized as staying within the path. That is, we describe winds summarizing multiple-day Lagrangian transports. More accurately, the path description for the curtain should be considered to represent a region 500 to 1000 km wide, allowing meandering, topographic effects, and transient eddies to have their effects on the overall flow. There is a strong resemblance of the path to the wind fields shown for the surface and the ~ 3.4 -km levels in Plates 1a and 1b. Additionally, there is a region of rising and overriding air, as seen in those plots. Recirculation and accumulation of pollutants are especially important in the South Africa anticyclone region [Tyson *et al.*, 1995], and the reader is asked to bear in mind that longer paths, or alternatively, lower effective winds, can produce similar results. The path of Figure 1 has positions marked out by letters that are approximately 800–900 km apart; these represent distances along the parcel track of about 1100 km (10° latitude); the compression is a partial description of the meandering of parcels following the variable daily weather. Assumed wind speeds are shown below; typical velocities are $\sim 7 \text{ m s}^{-1}$ in the first kilometers to 15 m s^{-1} aloft.

Winds and Clouds

Figure 2, described further below, illustrates a vertical view of this vertical ribbon that constitutes our two-dimensional model.

The horizontal labels on the top describe how far air has traveled since entering a polluting continent. The winds are put into the model using an idealized, time-independent velocity potential (stream function) and are, consequently, mass conserving. (Temporal variation of the winds would needlessly complicate the analysis). The model grid has a 2° ($\sim 220 \text{ km}$) horizontal resolution and 14 vertical levels, equally spaced through the troposphere to 12 km. There is sufficient wind shear in this part of the tropics that regions above about 10–12 km are very poorly represented in any case. Indeed, the airstreams from as low as 8 km and increasingly likely above 12 km above the equatorial region are more likely to follow a path toward the east rather than the west-southwesterly direction indicated by the general path.

Along the bottom are mnemonic location labels for a track that has significant variation in latitude and longitude. The regions *a* “entry” and *b* “southern” have not accumulated much persistent pollution along the track, while regions *c* “downwind” and *d* “override” mark a region with more accumulated ground-track distance and pollution. In these regions there tends to be a surface convergence and some lifting by narrow organized motion shown in Plate 1. The actual override winds in Figure 2 may be quite far downwind for the situation suggested by Plate 1. Remember, however, that in many situations there is more temporal variation, i.e., meandering and recirculation, than the Plate 1 streamlines suggest. Note also the weak reverse flow of a monsoon wind in the lowest kilometer from the Atlantic in toward near the equator. This was accomplished by devising a stream function flowing air from the right-hand side and producing a compensating mass sink under the override region (simulating flow out of the plane of model.) See also Singh *et al.*, [this issue] and Heikes *et al.* [this issue].

In the idealization of three-dimensional meteorology we are trying to simulate, winds become more organized along the paths *d* “override,” *e* “coast,” and *f* “Atlantic.” However, at approximately coast *e*, there are two possible coordinated motions. Conceptually, one might think of the plume as switching to the path marked “alternate” in Figure 1. While features of the modeling of the Great African Plume will follow this generalized

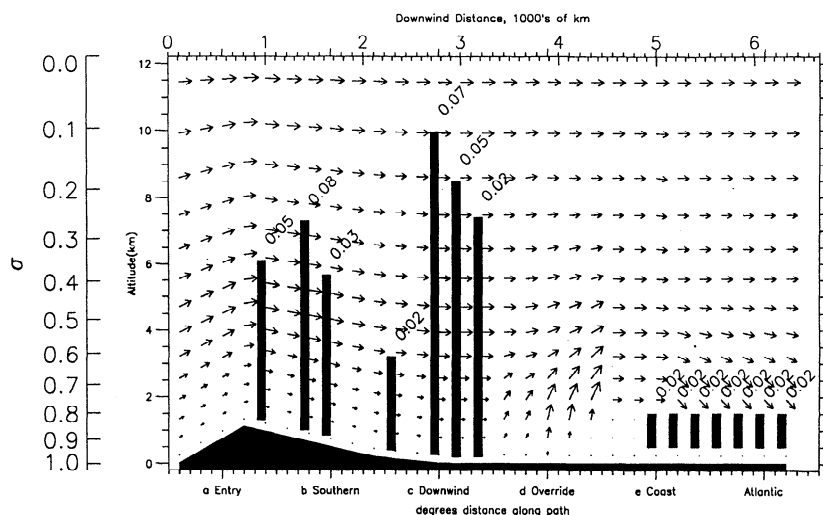


Figure 2. Wind fields used for the two-dimensional simulation, derived from an idealized stream function. Dark area at bottom shows the topography assumed. Top scale shows distance downwind from entrance of air to a burning continental region. Left-hand scale shows σ , the ratio of atmospheric pressure at a level to the surface pressure at the Earth's surface below. Vertical bars represent cloud updraft regions, with mass fluxes, in kilogram per second, and specified locations of updraft of outflows. Downdrafts were also specified, with originating levels approximately 0.5–0.66 the height of the outflow and with mass fluxes related by a Grell-type [Grell, 1993] proportionality factor, e , of 0.6.

trajectory, exact comparisons of data cannot be expected with this two-dimensional model.

Indeed, the level of abstraction acceptable for a two-dimensional model suggests our description may be appropriate for emissions originating from the highland savannas, cerrado, of Brazil and tending toward the moister, more convective regions of the Amazon Basin or the more southern subtropical cyclonic regions. The general motion is toward convergence regions of the equator or midlatitudes [Crutzen *et al.*, 1985; Loring *et al.*, this issue]. The latter are predominant in our three-dimensional results as analyzed to date. Roughly similar plumes can result when air takes the "alternate path" shown in Figure 1 and rounds the Cape of Good Hope. Analysis of our three-dimensional model, in progress, suggests that there are also plumes of air drawn off the Cape of South Africa into midlatitude eddies of the South Atlantic and the South Indian Ocean [Garstang *et al.*, this issue]. These should resemble our plume but likely differ in three ways: (1) length of accumulation of pollution, possibly lacking the recirculation of southern Africa; (2) more rapid dilution by more vigorous and variable winds; and (3) distortion of the patterns by more vigorous vertical wind shear.

In each of these cases, there is the feature of emissions over elevated grassy and agricultural lands, sustaining fierce surface heating during the day, followed by ascent and overriding of air over humid, typically cooler rain forest air, and eventually over cool marine boundary layers. Over the moist continental areas, deep cumulonimbus convection often gives a significant boost. This is a pattern typical of the continents bordering the Atlantic Ocean during the August-October maximum of total ozone. However, this pattern may hold less well for southeastern Asia and Indonesia. We speculate that these meteorological differences may help explain why strong ozone and CO accumulation found in the American-African tropics is less evident elsewhere [Fishman *et al.*, 1991].

Boundary Layer Mixing

The processes mixing material to the middle and troposphere are central to the phenomena we describe here; however, we have

kept their description simple. Plate 1 suggests a convergence region with interacting boundary layer and cloud features, but these details require further analysis. The basic process of lofting of polluted air from deeper dry continental boundary layers over shallower, moister, boundary layers has been described by Fishman *et al.* [1987] for the southeastern United States and the adjoining Atlantic, and our model has followed this description. The diel course of planetary boundary layer convective mixing over land has the classic [Kaimal *et al.*, 1976] variation shown in Figure 3a. Mixing rises during the daylight morning hours over the continent and maintains an afternoon peak until sunset. We chose the maximum mixing heights shown in Figure 3a guided by the maximum heights calculated from the MM5 model and tracer observations reported by Anderson *et al.* [this issue] that are described below. The MM5 model was run without a shallow convection parameterization, and so it yields one variable describable as a "mixing layer" height rather than two (the top one, cloud stirred) variables. A MM5 run made with considerable attention to the difficult problem of fair weather, nonprecipitating low clouds could suggest a dry-convective subcloud base rapidly mixed layer (probably lower than our MM5 and idealized layer, due to intercloud subsidence and a deeper, fair weather cloud nearly mixed layer (probably somewhat deeper than ours, due to the additional buoyancy effects of latent heat release). Our mixed layer top, paying no attention to shallow convection, should lie between the cloud base inversion and the greater height substantially mixed by fair weather clouds.

The diel variation of deep cloud convection has been less well characterized in the literature, so we have imposed a simpler, sinusoidal variation, maximizing at 1600 LT over land and 0400 LT over the ocean. Vertical transport by the clouds is accomplished by direct, nondetraining and nonentraining "pipes" which are identical with our three-dimensional transport parameterization, using the material transport described by Grell [1993]. These pipes create more localized output regions in the upper troposphere than the multiple pipes described by the Chatfield and Crutzen [1990] "Staubsauger" (vacuum cleaner) model for oceanic convection. Outside-cloud subsident transport

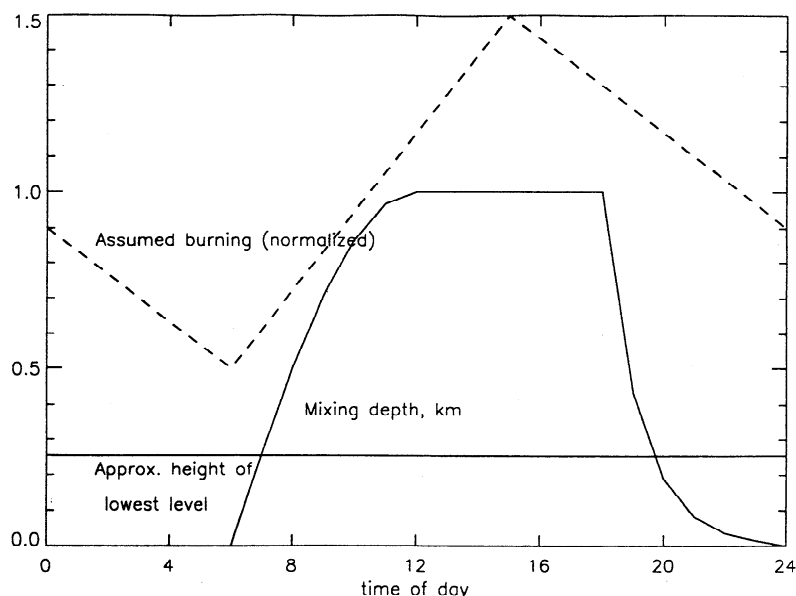


Figure 3a. Diel variation of continental planetary boundary layer (PBL) convection and burning emissions. The mixed layer depth is shown at a nominal 1 km, but in the mixed layer varies as in Figure 3, with an actual minimum depth of 0.25 km set by the resolution of the model and with an actual depth proportional to the normalized profile shown. Burning is assumed to rise rapidly to a maximum at 1500 LT and a minimum at 0500 LT.

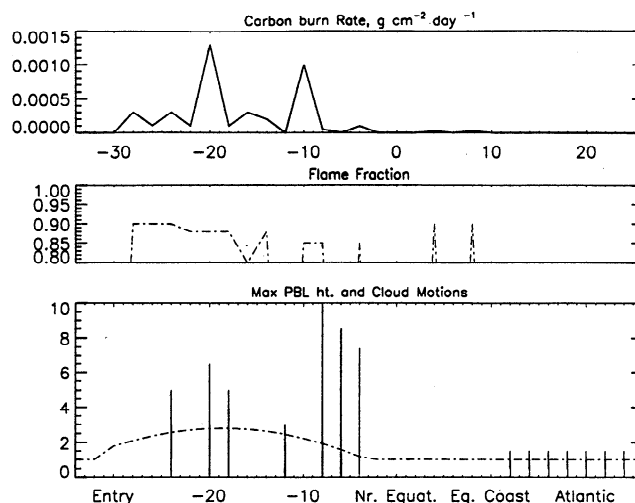


Figure 3b. Spatial variation of emissions intensities, i.e., C burn rate, in g cm⁻² d⁻¹, flaming fraction of the carbon burned (dimensionless), and planetary boundary layer height, in kilometer. Topography of the continental regions is shown, with PBL height added on.

in the same grid column spreads material slightly. As Figure 2 shows, this effect of narrow detrainment regions is broadened by having clouds with different output heights in neighboring grid cells. The choice of the depths of clouds, their geographical location along the model domain, and the associated mass fluxes are perhaps the most poorly determined choices in the model we present. The general locations we present are influenced strongly by our three-dimensional model results and, of course, by the underlying ECMWF analysis. Determination of the exact locations, the updraft tops, and mass fluxes are more delicate issues that deserve detailed meteorological studies in themselves for individual events [e.g., Wang *et al.* [this issue], Pickering *et al.* [this issue (b)], and supporting work]. We have instead been guided to choose cloud tops and mass fluxes that give reasonable CO concentration patterns in the lower and upper troposphere at the 10°S region and downwind and that also fall into the typical regions of intense convective mass flux we found in the MM5 results. Plate 1 illustrates that on October 2 there were separate convergence lines visible in southern Africa at approximately the 12°S parallel and the 25°E meridian, joining and leading to more equatorial convection in a northeastward line. This one simulation illustrates a broader point that deep convection occurs at various stages of a lower-tropospheric air mass progressively loading with more pollution. The unpublished satellite imagery used by Kendall *et al.* [1995] gives direct observational support to the view that cloud activity was frequent and variable during that first half of October 1992, reaching often down to 20°S to 25°S. There are locales of stronger convection and accompanying weaker, shallower convection, at progressively farther distances from entry to the polluting continent and correspondingly closer to the downwind ocean.

Methods

Emissions and Their Parameterization

Biomass burning emissions were estimated using a standard technique based on the mass of biomass burned per unit area, the nitrogen and carbon content of that biomass, and emission factors for a variety of trace gases and aerosol:

$$E_i = (\eta_i^{\text{flame}} f_i^{\text{flame}} + \eta_i^{\text{smolder}} f_i^{\text{smolder}}) N_i^{\text{ratio}} b^{\text{above ground}} f^{\text{burned}}$$

Here, the symbols represent

E_i : emission flux of chemical species i , molecules cm⁻² s⁻¹;

$\eta_i^{\text{flame}}, \eta_i^{\text{smolder}}$: emission factors for flaming and smoldering combustion (molecules) (species) molecules (C)⁻¹);

$f_i^{\text{flame}}, f_i^{\text{smolder}}$: fractions of fuel consumed by flaming and smoldering combustion (dimensionless);

N_i^{ratio} (for nitrogen-containing emissions): elemental ratio of N / C effective for biomass burned;

$b^{\text{above-ground}} f^{\text{burned}}$: carbon-burn-rate density, based on the areal density of biomass (converted to C, molecules (C) cm⁻² s⁻¹) and the fraction burned (dimensionless), obtained from Hao and Liu [1994].

The emission factors were based from the tabulation of Lobert [1991]. As in his estimation procedure, we parameterize the nitrogen-containing compounds on the basis of the nitrogen content of the fuel. We found that a N / C ratio of 2% gave good results for carbon monoxide, nitrogen oxide, and ozone concentrations, although such a ratio is perhaps 40% higher than literature values, especially for Brazilian savannas [Rodin and Bazilovich, 1967; Kaufman *et al.*, 1993]. This high ratio may represent N/C actually volatilized, may reflect high-N fuels (crop residues), or may simply be a bit too high. Additionally, areas without burning were allowed soil emissions of NO at a small background rate, 2×10^{-9} molecules cm⁻² s⁻¹ [e.g., Potter *et al.*, 1995]. Both the N / C ratio and the appropriate episodic NO emissions are sufficiently uncertain, and their effects in this large-scale model are commingled, that we did not pursue sensitivity studies. In addition, our later discussion points out a much larger difficulty with N mass balances which seems to have a separate

origin. More detailed mass-balance studies are indicated. For smoke aerosol we made a simple emission estimate of the total mass emitted, using the emission factors for Africa derived by *Anderson et al.* [this issue].

Figure 3a shows our approximation of the diel cycle of biomass burning emissions, emphasizing a typical coincidence of emission and vertical mixing. The diel pattern of combustion maximizes in the afternoon, according to most field observations and inferences of satellite imagery of large fire areas which are visible in analyzed satellite imagery. *Langaas* [1993] describes a western African example of uncontrolled fires. E. Prins (University of Wisconsin personal communication, 1995) finds a maximum from geostationary imagery of 1300-1600 LT in Bolivia. The exact form of the variation for all fires seems poorly known. The surface observations reported that *Langaas* work suggests that the maximum time has a factor of 8 more burning than the minimum, maximizing in the middle of the day; additionally, studies using remote sensing suggested only 3 times more fires signal at 2200 than at 1500 LT. A previous study using samples at local midnight suggested that the horizontal pattern of fires for the continent of Africa could be seen at night and was very similar to daytime patterns [*Cahoon et al.*, 1992]; the authors suggested on this basis that "fires are left to burn uncontrolled and as the fire imagery shows, fire frequency may not be so strongly diurnal as commonly believed." *Langaas* [1993] counters that relative humidity and wind speed should also modulate fire activity even for large, long-lasting fires. In summary, we have selected a very modest factor of 3 variation from maximum to minimum. Probably a larger factor applies. Our assumed spatial patterns of burning and emission strengths (which have the same variation day and night) are discussed below.

We have relied on conventional estimates for biomass burning, based on statistics compiled from a variety of country reports by agencies such as the Food and Agriculture Organization [*Hao and Liu*, 1994]. These are climatological estimates, thought to be valid for several years' averaging times, but not necessarily for the 1992 period during which we have confirming airborne concentration estimates of the same pollutants. Specific emission estimates for this period are beginning to appear [*Kendall et al.*, 1995; *Scholes et al.*, this issue]. These estimates are based on more detailed characterization of the ambient vegetation available for fuel and on interpretations of satellite products like AVHRR thermal emission fields or higher-resolution interpretations of burning ash scars. These independent methods of burning estimation appear to give much smaller emissions, perhaps more than a factor of 3 lower than the *Hao and Liu* levels, beyond the variation expected from year to year in response to weather variation. Our idealized simulations constitute an initial attempt at deciding which estimates are most appropriate: if the *Hao and Liu* [1994] emissions are greatly off (more than a factor of 2, which is quite possible), both the two-dimensional and the three-dimensional models, which ventilate a major product like CO, should have noticeable disparities in simulated concentrations.

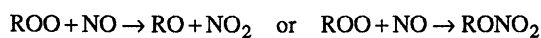
While the general levels resemble the *Hao and Liu* [1994] averages, we have chosen to concentrate the emissions into concentrated regions (see Figure 3b) resembling the 2°-4° wide areas shown in Plate 3 and by *Kendall et al.* [1995] and *Justice et al.* [this issue] on the basis of remote sensing. This is important for reasons described by *Chatfield and Delany* [1990]: ozone production and NO_x loss are dependent on the product of concentrations of reactants and do not respond linearly to spatial averaging. Regions of concentrated concentrations were also sampled by the TRACE A DC-8. The emissions described in

Figure 3b do repeat the diel cycle at each spatial location, so as to simplify analysis within the constraints of a two-dimensional model.

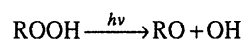
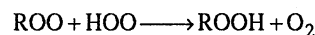
Chemical Mechanism

The chemical mechanism we chose to use is given in Table 1. The reaction scheme is an outgrowth of one described by *Chatfield and Delany* [1990] and is very close to one whose results are published in a model intercomparison made by the Intergovernmental Panel on Climate Change [*Olson et al.*, 1995]; the version used lacks isoprene reactions (see below). Models in the intercomparison were subjected to a large variety of test problems, and this mechanism-model combination proved typically to provide results similar to the majority of the models.

The mechanism deals directly with the fact the prime fate of most peroxy radicals in of the Earth's atmosphere is not reaction with NO,



Because of the low NO concentrations in the background lower troposphere, there are only fragmentary guides in the chemical review literature on how to model the reactions in detail. The *Madronich and Calvert* [1990] work on permutation reactions of organic peroxy radicals is only now being updated by new assessments largely unavailable in reviewed literature (W. Stockwell, personal communication, 1994). Unpublished simulations by Chatfield with the Madronich "master mechanism" in a variety of tropospheric low-NO settings suggest that the largest fate of organic peroxy radicals is with hydroperoxy radicals except in atmospheres of unusual composition. For this reason, when considering large-scale chemistry, we have avoided the complexities of a permutation-reaction parameterization and followed the philosophy detailed by *Chatfield and Delany*. Briefly, the reactions of organic peroxy radicals and organic peroxides are considered according to this formalism:



Reactions of this sort have been introduced for all reactions in which organic peroxy radicals are produced. This reaction set does tend to produce large concentrations of organic hydroperoxides, which are not removed effectively by rain, as is hydrogen peroxide. The mechanism intentionally treats only low chain-length organic emissions, C₂ and C₃, and began from the *Lurmann et al.* [1986] mechanism, and thereby omits consideration of organic nitrates, which are produced from heavier hydrocarbons. In doing so, it does not allow for consequential nitrogen storage in these species. The small quantity of higher-mass alkanes emitted from fires [*Lobert*, 1991] was lumped in with propane in the emissions, complicating the propane comparisons slightly. This characteristic of the model appears adequate since organic nitrate compounds in the atmosphere are not observed to carry much nitrogen, with the notable exception of PAN, which we include [*Roberts*, 1995].

Future studies, especially of regions with active arboreal vegetation, deserve an isoprene mechanism. The most vegetated African area we compare to, that is, the most equatorial in TRACE A, was at the northern extension of flight 10, near Lake

Table 1. Reactions Describing Ozone Production in the Polluted and Remote Troposphere

Reactants	Photolysis/Troe?	Products	Preexponential	T _{Arrhenius}	T _m
NO ₂	<i>j</i> →	NO + O ₃			
NO + O ₃	→	NO ₂ + O ₂	0.200E-11	1400.	
NO ₂ + O ₃	→	NO ₃ + O ₂	0.120E-12	2450.	
NO + NO ₃	→	2.00 NO ₂	0.150E-10	-170.	
NO ₃ + NO ₂	<i>Tr</i> →	N ₂ O ₅			
N ₂ O ₅	<i>Tr</i> →	NO ₃ + NO ₂			
NO ₂ + NO ₃	→	NO + NO ₂ + O ₂	0.450E-13	1260.	
NO ₃	<i>j</i> →	.150 NO .850 + NO ₂ .850 + O ₃			
NO ₃ + HO ₂	→	HNO ₃ + O ₂	0.410E-11		
O ₃	<i>j</i> →	O1D			
O1D + H ₂ O	→	OH + OH	0.220E-09		
O1D + M	→	O ₃	0.140E-10	-110.	
O1D + M	→	O ₃	0.670E-11	-70.	
OH + NO ₂	<i>Tr</i> →	HNO ₃			
HNO ₃	<i>j</i> →	NO ₂ + OH			
HNO ₃ + OH	→	NO ₃	0.140E-13	-650.	
CO + OH	→	HO ₂	0.150E-12		
CO + OH + M	→	HO ₂	0.369E-32		-1.
O ₃ + OH	→	HO ₂ + O ₂	0.160E-11	940.	
NO + HO ₂	→	NO ₂ + OH	0.370E-11	-250.	
HO ₂ + NO ₂	<i>Tr</i> →	HNO ₄			
O ₃ + HO ₂	→	OH 2.00 + O ₂	0.110E-13	500.	
HO ₂ + HO ₂	→	H ₂ O ₂ + O ₂	0.230E-12	-600.	
HO ₂ + HO ₂ + M	→	H ₂ O ₂	0.170E-32	-1000	
HO ₂ + HO ₂ + H ₂ O	→	H ₂ O ₂	0.322E-33	-2000	
H ₂ O ₂ + OH	→	HO ₂ + H ₂ O	0.290E-11	160.	
H ₂ O ₂	<i>j</i> →	OH + OH			
HNO ₄	<i>Tr</i> →	HO ₂ + NO ₂			
HNO ₄ + OH	→	NO ₂ + H ₂ O + O ₂	0.130E-11	-380.	
HCHO	<i>j</i> →	2.00 HO ₂ + CO			
HCHO	<i>j</i> →	CO + H ₂			
HCHO + OH	→	HO ₂ + CO + H ₂ O	0.100E-10		
HCHO + HO ₂	→	AHO ₂	0.970E-14	-625.	
AHO ₂ + HO ₂	→	ACO ₂	0.560E-14	-2300	
AHO ₂ + AHO ₂	→	2.00 ACO ₂ 2.00 + H ₂ O 2.00 + O ₂	0.570E-13	-750.	
ACO ₂ + OH	→	HO ₂ + H ₂ O	0.450E-12		
NO ₃ + HCHO	→	HNO ₃ + HO ₂ + CO	0.580E-15		
ALD2 + OH	→	MCO ₃ + H ₂ O	0.600E-11	-250.	
ALD2 + NO ₃	→	HNO ₃ + MCO ₃	0.140E-11	1900.	
ALD2	<i>j</i> →	MO ₂ + HO ₂ + CO			
ALD2	<i>j</i> →	CH ₄ + CO			
MCO ₃ + NO ₂	<i>Tr</i> →	PAN			
PAN	→	MCO ₃ + NO ₂	0.400E+17	13600	
MCO ₃ + NO	→	MO ₂ + NO ₂	0.240E-10		
MO ₂ + NO	→	HCHO + NO ₂ + HO ₂	0.420E-11	-180.	
CH ₄ + OH	→	MO ₂ + H ₂ O	0.290E-11	1820.	
C ₂ H ₆ + OH	→	ETO ₂ + H ₂ O	0.870E-11	1070.	
C ₃ H ₈ + OH	→	.310 A3O ₂ .690 + B3O ₂	0.110E-10	700.	
ETO ₂ + NO	→	ALD2 + HO ₂ + NO ₂	0.450E-11		
A3O ₂ + NO	→	.036 A3N2 1.97 + RCHO	0.450E-11		
A3O ₂ + NO	→	1.97 NO ₂ 1.97 + HO ₂	0.870E-11		
B3O ₂ + NO	→	.04 B3N2 .960 + ACET .960 + NO ₂ .960 + HO ₂	0.850E-11		
ACET + OH	→	ACE2	0.160E-10		
ACET	<i>j</i> →	MCO ₃ + MO ₂			
ACE2 + NO	→	MCO ₃ + HCHO + NO ₂	0.870E-11		

Tanganyika at 10°–12°S, discussed below in our “source characterization” section. Here, average isoprene and propene (technique) [Blake *et al.*, this issue] were 95 and 322 ppt at 500 feet altitude; at 1000 feet, well within the boundary layer, the isoprene was down to 34 ppt average and the propene at 350 ppt. This threefold to tenfold difference in comparison to propene (alone!) indicates that our simulated chemistry is not too perturbed by the lack of isoprene, even given isoprene’s higher reactivity. Perhaps vegetation is just recovering as the October rains return, and other situations would require more isoprene. The expected effect of adding isoprene would be for slightly increased ozone

concentrations over what we simulate. The effect on PAN, the prime organic reservoir of nitrogen, would be smaller. Isoprene, with one methyl group, is an inefficient precursor for PAN.

Reaction rate estimates were chosen by the following rules: The Jet Propulsion Laboratory (JPL) report series [DeMore *et al.*, 1994] were used if a reaction was reported there. The broader coverage of tropospheric reactions made the International Union of Pure and Applied Chemistry (IUPAC) recommendations the next choice [Atkinson *et al.*, 1992]. (For technical reasons these evaluations lag the JPL reports slightly.) Oxidized organics reactions not found elsewhere followed the reviews of Atkinson

TABLE 1. (continued)

Reactants	Photolysis/Troe?	Products	Preexponential	T _{Arrhenius}	T _m
RCHO + OH		RCO ₃ + H ₂ O	0.600E-11	-250.	
RCHO + NO ₃	→	HNO ₃ + RCO ₃	0.140E-14		
RCO ₃ + NO ₂	Tr→	PAN			
OH + MOH	→	HO ₂ + HCHO	0.670E-11	600.	
OH + BOH	→	HO ₂ + ALD2	0.700E-11	235.	
MO ₂ + MO ₂	→	1.40 HCHO .800 + HO ₂ .600 + MOH + O ₂	0.250E-12	-190.	
ETO ₂ + ETO ₂	→	1.60 ALD2 1.20 + HO ₂ .400 + BOH	0.150E-12	270.	
A3O ₂ + A3O ₂	→	1.20 RCHO 1.20 + HO ₂ .400 + ALD2 + R3OH	0.300E-12		
HO ₂ + MO ₂	→	MP + O ₂	0.380E-12	-800.	
HO ₂ + ETO ₂	→	ETP + O ₂	0.650E-12	-650.	
HO ₂ + A3O ₂	→	RA3P + O ₂	0.300E-11		
HO ₂ + MCO ₃	→	MAP + O ₂	0.300E-11		
HO ₂ + RCO ₃	→	RP + O ₂	0.300E-11		
ETHE + OH	Tr→	EO ₂			
PRPE + OH	Tr→	PO ₂			
EO ₂ + NO	→	NO ₂ + GLYC	0.420E-11	-180.	
PO ₂ + NO	→	NO ₂ + ALD2	0.420E-11	-180.	
ETHE + O ₃	→	2.00 HCHO .800 + CHO ₂ .240 + HO ₂ .840 + CO	0.600E-14	2630.	
ETHE + O ₃	→	.120 CH ₄ .420 + H ₂ O 2.00 + H ₂	0.600E-14	2630.	
PRPE + O ₃	→	1.57 HCHO 1.50 + ALD2 .600 + CHO ₂	0.220E-14	1900.	
PRPE + O ₃	→	.600 CRO ₂ .690 + HO ₂ .637 + MO ₂	0.220E-14	1900.	
PRPE + O ₃	→	.270 OH .990 + CO	0.220E-14	1900.	
CHO ₂ + NO	→	HCHO + NO ₂	0.700E-11		
CHO ₂ + NO ₂	→	HCHO + NO ₃	0.700E-12		
CHO ₂ + H ₂ O	→	ACO ₂	0.400E-17		
CRO ₂ + NO	→	ALD2 + NO ₂	0.700E-11		
CRO ₂ + NO ₂	→	ALD2 + NO ₃	0.700E-12		
CRO ₂ + H ₂ O	→	ACTA	0.400E-17		
GLYC + OH	→	.500 GCO ₃ .500 + GLYX	0.160E-10		
GPAN	→	GCO ₃ + NO ₂	0.112E+17	13330	
GCO ₃ + NO ₂	→	GPAN	0.470E-11		
GCO ₃ + NO	→	NO ₂ + HO ₂	0.420E-11	-180.	
GLYC	j→	HCHO 2.00 + H ₂ O			
EO ₂ + EO ₂	→	1.20 GLYC 1.20 + HO ₂ .400 + EOH .400 + ALD2	0.500E-13		
PO ₂ + PO ₂	→	1.20 RCHO 1.20 + HO ₂ .400 + ALD2 + R4OH	0.500E-13		
HO ₂ + EO ₂	→	EP + O ₂	0.300E-11		
HO ₂ + PO ₂	→	PP + O ₂	0.300E-11		
PRPE + NO ₃	→	PRN1	0.420E-14		
PRN1 + HO ₂	→	PRPN + O ₂	0.300E-11		
PRN1 + NO	→	2.00 NO ₂ + HCHO	0.420E-11	-180.	
CHO ₂ + HCHO	→	OZID	0.136E-13		
CHO ₂ + ALD2	→	OZID	0.136E-13		
CRO ₂ + HCHO	→	OZID	0.136E-13		
CRO ₂ + ALD2	→	OZID	0.136E-13		
OH + MP	→	.500 MO ₂ .500 + HCHO .500 + OH	0.100E-10		
OH + ETP	→	.500 ETO ₂ .500 + ALD2 .500 + OH	0.100E-10		
OH + RA3P	→	.500 A3O ₂ .500 + RCHO .500 + OH	0.100E-10		
OH + MAP	→	.500 MCO ₃ .500 + HCHO .500 + OH	0.100E-10		
OH + EP	→	.500 EO ₂ .500 + GLYC .500 + OH	0.100E-10		
OH + PP	→	.500 PO ₂ .500 + RCHO .500 + OH	0.100E-10		
OH + RP	→	.500 RCO ₃ .500 + ALD2 .500 + OH	0.100E-10		
MP	j→	OH + HO ₂			
ETP	j→	OH + HO ₂			
RA3P	j→	OH + HO ₂			
MAP	j→	OH + HO ₂			
EP	j→	OH + HO ₂			
PP	j→	OH + HO ₂			
RP	j→	OH + HO ₂			
NH ₃ + OH	→	NO ₂ + H ₂ O	0.330E-11	900.	
HNO ₄	j→	HO ₂ + NO ₂			
H ₂ + OH	→	HO ₂	0.550E-11	2000.	

Read 0.200E-11 as 0.200 x 10⁻¹¹. For Troe reactions, Troe (Tr) and photolysis reactions (j) see original references as listed in text. Column labeled *m* gives the power of *T* in rate expression, *T_m*.

[1994]. Deposition velocities were set to commonly accepted values, as described by Chatfield and Delany [1990]. Clear-sky photolysis rates are used throughout the domain. (As an aside, one way in which the model could be improved would be the inclusion of cloud effects on photolysis rates; we will reserve these effects until we may also calculate the effects of smoke on photo rates

below 4 km. Both effects should decrease the reactivity of the boundary layer air in the photochemically most reactive regions; we suspect that the smoke aerosol effects will be most important.)

The treatment of heterogeneous scavenging was simple. Very soluble gases like HNO₃ and H₂O₂ were removed completely in both updrafts and saturated downdrafts. Aerosol particle mass was

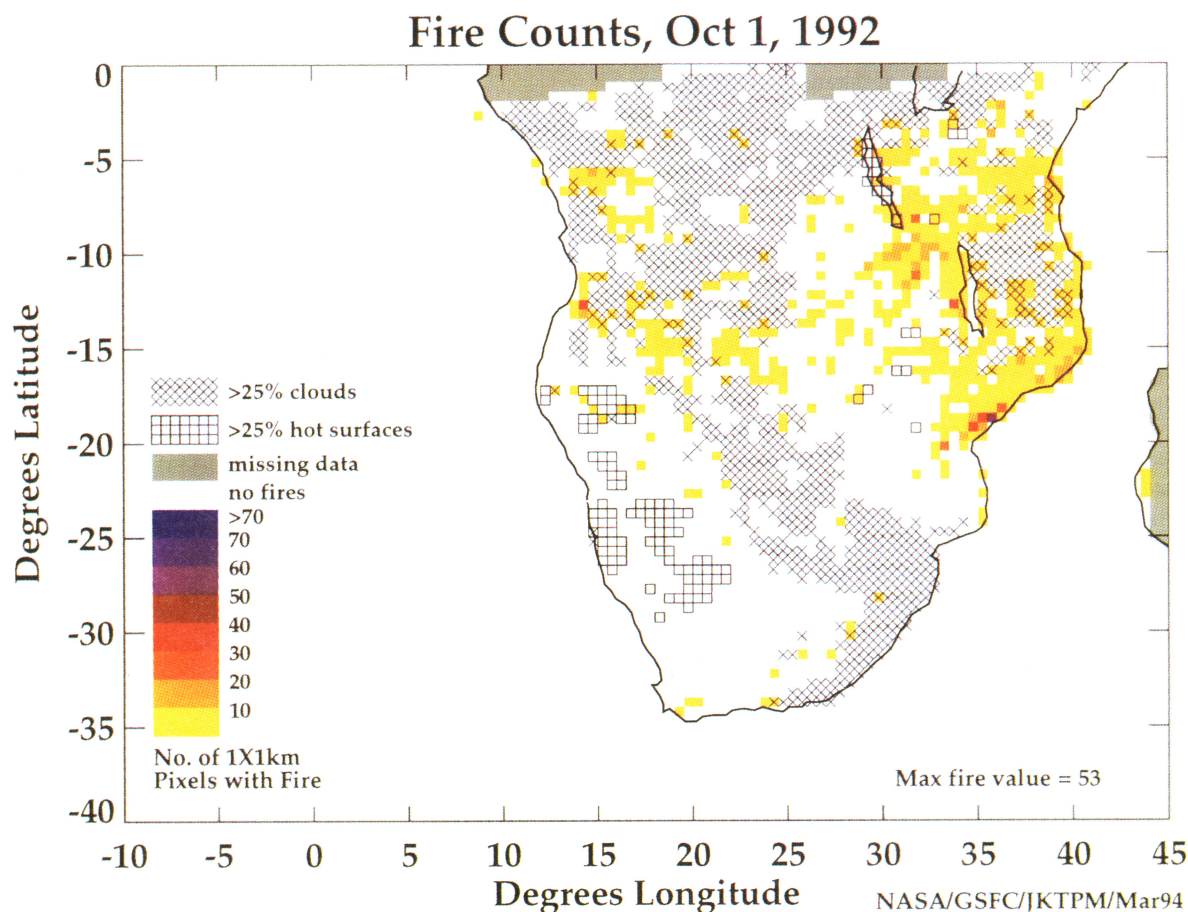


Plate 3. Fire counts and cloud prevalence for October 1, 1992 [Justice *et al.*, this issue]. Fire counts are interpreted from regions of high thermal emission and aid in a more detailed computation of biomass burned. Cloudy regions, >25% cloud cover (hatched), are also of interest; compare October 1 clouds and October 2 convergence and cloud fields in Plate 1; the days had similar meteorology.

80% removed, and only in updrafts, corresponding to an assumption that larger submicron and supermicron particles both constitute most all of the mass of the aerosol and make excellent condensation nuclei. This 20% transmission of mass was suggested by a series of papers initiated by Flossmann *et al.* [1988], which have continued to suggest that a very large proportion of the aerosol by mass is removed in deep convective systems. In future studies we expect to estimate the mass removal parameter. No below-cloud scavenging of gases or particles was treated, since convective rain shafts tend to affect a very small portion of the ~200-km grid areas we simulate and a portion very likely to be cleaned by updraft removal.

Dry deposition rates were as described by Chatfield and Delany [1990]. Ozone deposition over water was reduced. An aerodynamic resistance as well as an intrinsic surface-related resistance were employed [see Seinfeld, 1986, chapter 16].

Results and Discussion

Varieties of Biomass Burning Plumes

Qualitative features. Results of the idealized-plume simulation are shown in Plates 4-8. The contours shown represent atmospheric gases and aerosol mass at 1600 LT 10 days after the beginning of the simulation, at which point the model has reached

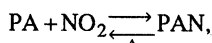
a daily repeating steady state. Initial conditions for the situation are visible as the boundary condition on the left side of the plots. While extensive biomass burning plumes are found for all species, there are great differences in the patterns of the plumes.

In this section, we describe the qualitative behavior of these and other species; in the next subsection we find generally good quantitative comparisons with the TRACE A data, with the signal exception of nitric acid. First, note that the CO plume (Plate 4) shows many similarities to the snapshot of the Great African Plume simulated in three dimensions (Plate 2). High concentrations of CO extend up through the 4-km region of highest dry-convective mixing, and layers of even higher CO extend both eastward and westward from the coastline. Pockets of very high values over 250 ppb are visible in the two-dimensional simulation; however, remember that Plate 4 intentionally reflects specifications of regions of intense emissions for reasons discussed below. Consequently, concentrations rise somewhat higher near the ground, 220 ppb, while the high 200 ppb concentrations of Plate 2 are somewhat more restricted. Midtropospheric values in the near-equatorial region of 80-140 ppb appear in both figures, suggesting that the integrated effects of CO emission rates, horizontal ventilation, and cloud transport are similarly modeled in the two-dimensional and three-dimensional models. While the high concentrations do not move far east in the three-dimensional above 7 km, other three-

dimensional analysis suggests that they have simply turned out of the plane of depiction; some of the high values of a “C-shaped” CO profile are visible in the high concentrations in the southeast and east panels of the Figure 1 cross sections. The two-dimensional model, Plate 4, has a relative minimum in the plume of 100 ppb at 4 km over the ocean. This is an artifact of the model construction but nevertheless illustrates a kind of lamination of plumes that is often observed.

A qualitative overview of the plume shapes will give a brief tour of the different possible meanings of the phrase “biomass burning plume.” In assessing these remarks, the reader may check the patterns in figures, noting that a similar, linear scale is used for all the contour plots. The aerosol mass (AERMS) plume of Plate 5 is the shallowest and thinnest of all the modeled plumes and extends with little dilution for a thousand kilometers into the eastern equatorial Atlantic, overriding above the “monsoon” oceanic inflow layer. Its limited vertical extent results directly from the simulation assumptions: all aerosol mass is treated as primary emission, and 80% of the aerosol mass is removed when entrained into the updraft of any cloud. Very low-concentration plumes exiting from cloud tops might be more realistic, but they are currently somewhat impractical to simulate. The deeper, layered CO plume of Plate 4 is of a primary emission with very slow chemical reaction and no cloud removal and displays peaks in both the lower and the upper troposphere, a “C-shaped” concentration profile with altitude. It is the simplest atmospheric trace of biomass burning influence. Acetylene (C₂H₂) in Figure 4 shows a very similar pattern. Especially C₂H₂ and CO are approximately unreactive and insoluble within the time periods considered. The NO_x pattern (Plate 6) is one of a very short lived species, with intense hot spots near sources (poorly resolved at 2° resolution) and localized maxima at cloud-output regions and up to 10° downwind. The modeled nitric acid plume is very similar to the aerosol mass plume, since HNO₃ is simulated as removed completely in cloud updrafts and downdrafts. Note that there are additions of small maxima trailing from the cloud-detachment regions marked by the NO_x detrainment regions.

Propane, C₃H₈ (Plate 7), has greater transience than CO or C₂H₂ in the lower troposphere due to its faster few-day reactive timescale. Propane spreads further in the cold upper troposphere due to faster winds and a high activation energy, which slows its reaction with hydroxyl. Peroxy acetyl nitrate, PAN, shows plumes essentially opposite to those of aerosol mass, persisting only in the upper troposphere. The great effects of cold temperatures in extending the decomposition lifetime of PAN from hours to months in the upper troposphere explains this inverted behavior. More careful inspection of the PAN plots suggests both “positive” and “negative” plumes. Positive plumes in the upper troposphere are directly linked to regions of concentrated emissions in the lower troposphere, where precursor organics and nitrogen dioxide are both concentrated. A negative plume (green values, corresponding to lower-than-ambient concentrations) is linked to a region near “override”, 2600 km, where the lower troposphere is relatively clean of fresh emissions. This is a region where CO persists, but both organics and NO_x are reduced. Since PAN chemistry in the lower troposphere may be represented



where PA represents the peroxy acetyl radical (formed primarily as an oxidation product of reactive organic emissions). Consequently, the concentrations of PAN, where PAN has a few hour lifetime, the active-chemistry regions, should be

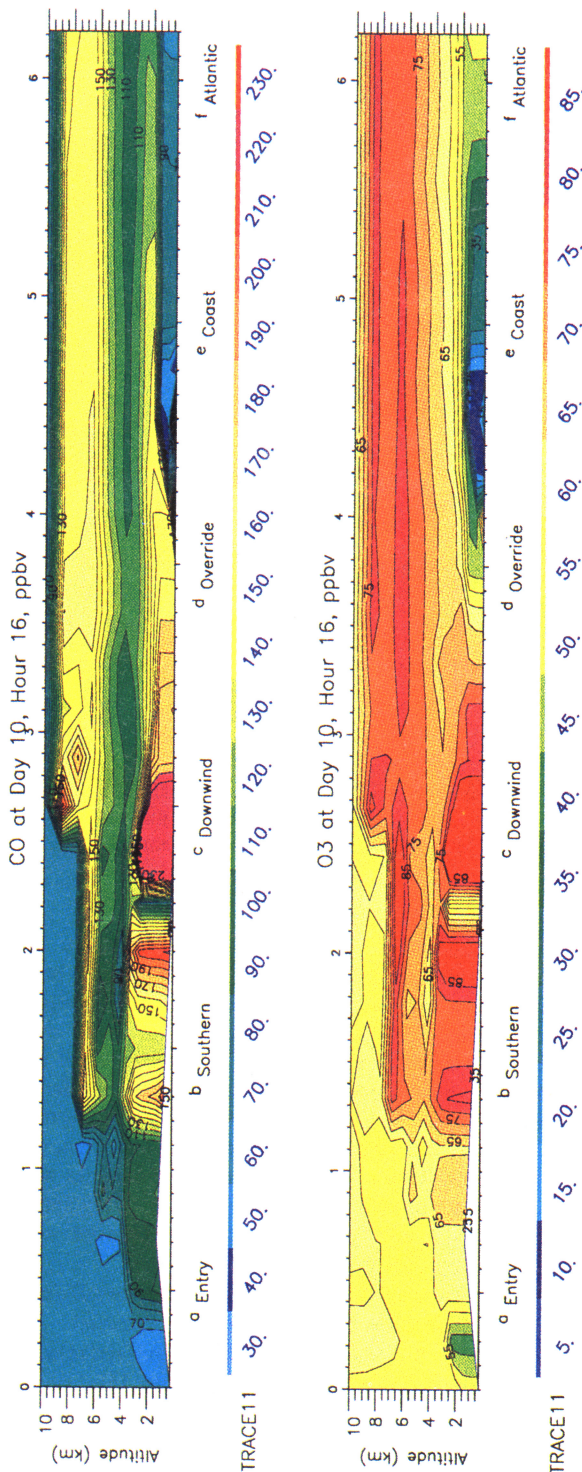


Plate 4. Contour plots of CO and O₃ concentrations in the idealized version of the Great African Plume, in parts per billion by volume (molecular ratio). Local time of simulation for this and subsequent plots is 1600.

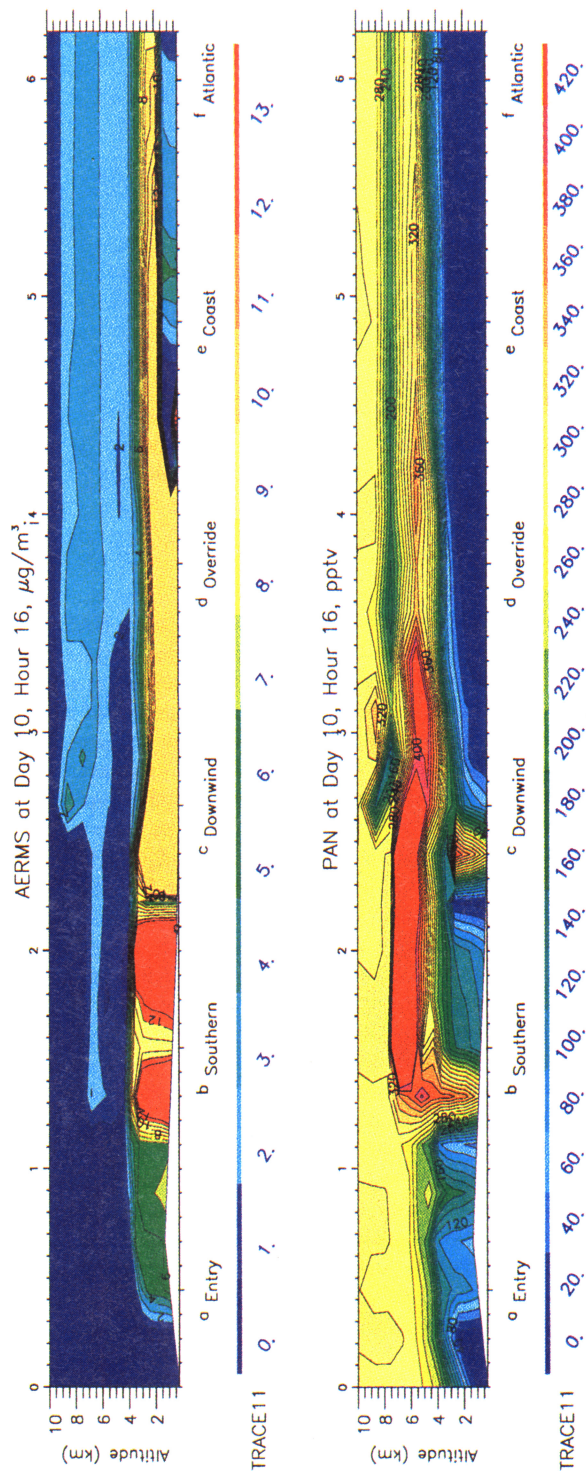


Plate 5. Aerosol mass ($\mu\text{g m}^{-3}$) and PAN, parts per trillion. Aerosol mass contours are truncated above $14 \mu\text{g m}^{-3}$ for legibility; our maxima reach approximately $60 \mu\text{g m}^{-3}$ near 2000 elapsed kilometers.

quadratically related to pollution intensity of relatively short lived species, being proportional to $k_{\text{PA}+\text{NO}_2}[\text{PA}][\text{NO}_2]$. This will be called the “quadratic pollutant concentration effect” and figures in our quantitative comparisons below.

Another feature evident in the PAN plumes is a set of concentration maxima and minima seen downstream in the plume. Similar features are seen in other plots, particularly the radical concentrations OH and HO₂, seen in Figure 5. These are traces of previous days’ afternoon convection, either cloud convection, as for PAN, or boundary layer and cloud convection, for the radicals.

Some of the features of the simulation are direct consequences of the formulation of an idealized, two-dimensional model. For example, since the simulation is two dimensional, once an unreactive species enters the flow, it will persist in all the downwind field, unless there is substantial effect of vertical mixing and transport. This means that plumes tend to be static, persistent features, not subject to meandering behavior found in true three-dimensional plumes. The diel variation of flaming emissions and boundary layer mixing introduce some variation in this model, but the effects are greatly smoothed. An inspection of the contour plots and the distribution of convection shows that cloud ventilation and wet removal dominate the downwind variation of tracers. In these 1600 LT plots, with many hours of vigorous boundary layer mixing, the effects of dry deposition are more difficult to note; deposition rates are controlled by the standard subgrid surface-layer formulae. If there were more thin levels calculated near the surface, the effects of deposition on the profile over the continental regions would be clearer.

The coincidence of burning, boundary layer mixing, and cloud venting in the afternoon efficiently mixes fresh emissions from the surface, aiding somewhat the “mix-and-cook” chemistry, i.e., high ozone production from diluted, freshly emitted NO_x [Chatfield and Delany, 1990], while preventing near-surface concentrations from reaching extreme values very often.

Emissions and Airborne Concentration Distributions

Comparisons to TRACE A. Return now to the consideration of the contour diagrams, Plates 4-8; we will attempt comparisons of this diel-steady-state, idealized model with highly situation-specific observations of air composition over southern Africa and the Atlantic Ocean made by the NASA DC-8 investigators in TRACE A during early October 1992. Exact agreements are not to be expected, since the aircraft observations should vary more widely, depending on the vagaries of varying fire emissions and weather patterns, but general patterns and concentration levels can be expected to show some similarities. Positions along the axis are to be interpreted primarily as distances downwind from an initial entry to the burning lands, but we suggest a good correspondence from the letter markings in Figure 1. Our MM5 results and the Garstang et al. [this issue] analysis suggest a meandering, sometimes recirculating character to this northward drift. Left of this region is to be interpreted as entry of air toward central South Africa. Bear in mind also that the intensity of emissions and vertical convective mass fluxes have been estimated in the model to obtain reasonable but not exact agreement with lower-tropospheric CO measurements. Since other species have different background concentrations, cloud removal processes, and chemical lifetimes, they tend to provide independent checks.

Aerosols. The main aerosol plume extended to 3 km except in regions of high boundary layers and topography, where it extends to 4 km. It is also lifted over a marine boundary layer to make a top at 4 km. This behavior compares very well with the

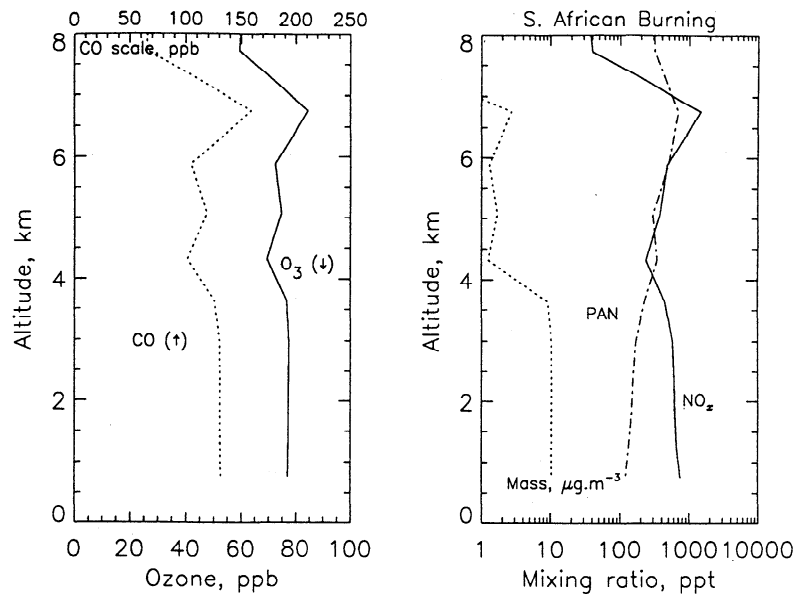


Figure 4a. Simulated upwind region profiles of ozone, carbon monoxide, PAN, and NO_x from the model calculation over the southern African plateau. Refer also to contour plots above. Local time is 1600 for this and subsequent plots.

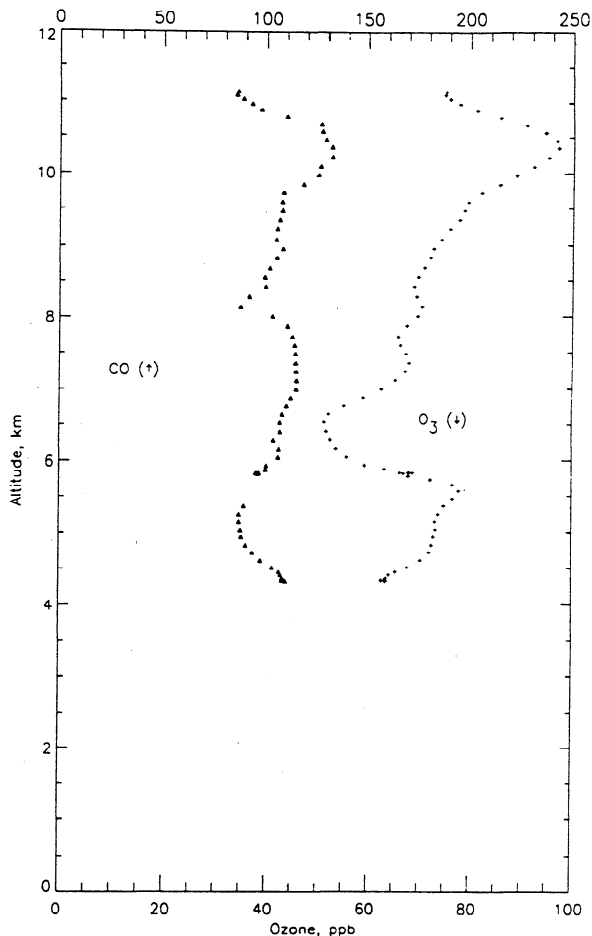


Figure 4b. Observations of ozone and carbon monoxide made on flight 9 near Johannesburg at 1530 UT, approximately 1730 LT, in a region that had just begun to accumulate pollution.

observations reported by Anderson as interpretations of the NASA Langley UV DIAL (ultraviolet differential absorption lidar) lidar backscatter cross sections [Anderson *et al.*, this issue] and in situ measurements (flight 13, at $\sim 8^{\circ}\text{S}$, 9°E); interpretations of the backscatter parameters are continuing so as to refine the aerosol mass density estimates, but the $12\text{--}14\ \mu\text{g m}^{-3}$ values we simulated are in reasonable agreement with the current Anderson estimates. The highest concentrations we simulate, near $60\ \mu\text{g m}^{-3}$, are near the values found by Anderson in a plume they sampled in flight 10 (their Figure 12). Our upper troposphere values range from 1 to $3\ \mu\text{g m}^{-3}$, originating from detraining clouds. Values derived from the observations of that flight appear to be smaller, around $1\ \mu\text{g m}^{-3}$, or even lower. Note, however, that we used their emission factors, which were, in turn, derived from near-source concentration measurements, albeit by different methods.

These calculated aerosol concentrations (and analysis of observed concentrations) are extremely high, nearly an order of magnitude larger than $0.1\text{--}0.2\ \mu\text{g m}^{-3}$ mass loadings thought to characterize the free troposphere [Patterson *et al.*, 1980]. While we used a most accepted value for aerosol mass transmission by clouds of 20%, a much smaller figure may be appropriate, e.g., 5%. It is relatively easy to scale aerosol concentrations above about 5 km: an early run of the model using a 10% transmission of mass (a value consistent with Anderson *et al.*, this issue); the upper tropospheric concentrations were indeed lower by a factor of 2.

The model results illustrate the basic hypothesis that dry convective process emplaces large concentrations of aerosol in the tropical midtroposphere, but when one rises in the atmosphere to observe at a level most influenced by precipitating clouds, not shallow convection, the concentrations drop precipitously. The characteristic vertical profile of particle number that Anderson *et al.* [this issue] show for outflow or plume air over the Atlantic (their Figure 14) has the same 2- to 4.5-km structure of our profile for aerosol mass (our Plate 5). Admittedly, our simulation of the aerosol plume is crude, reflecting observed subcloud

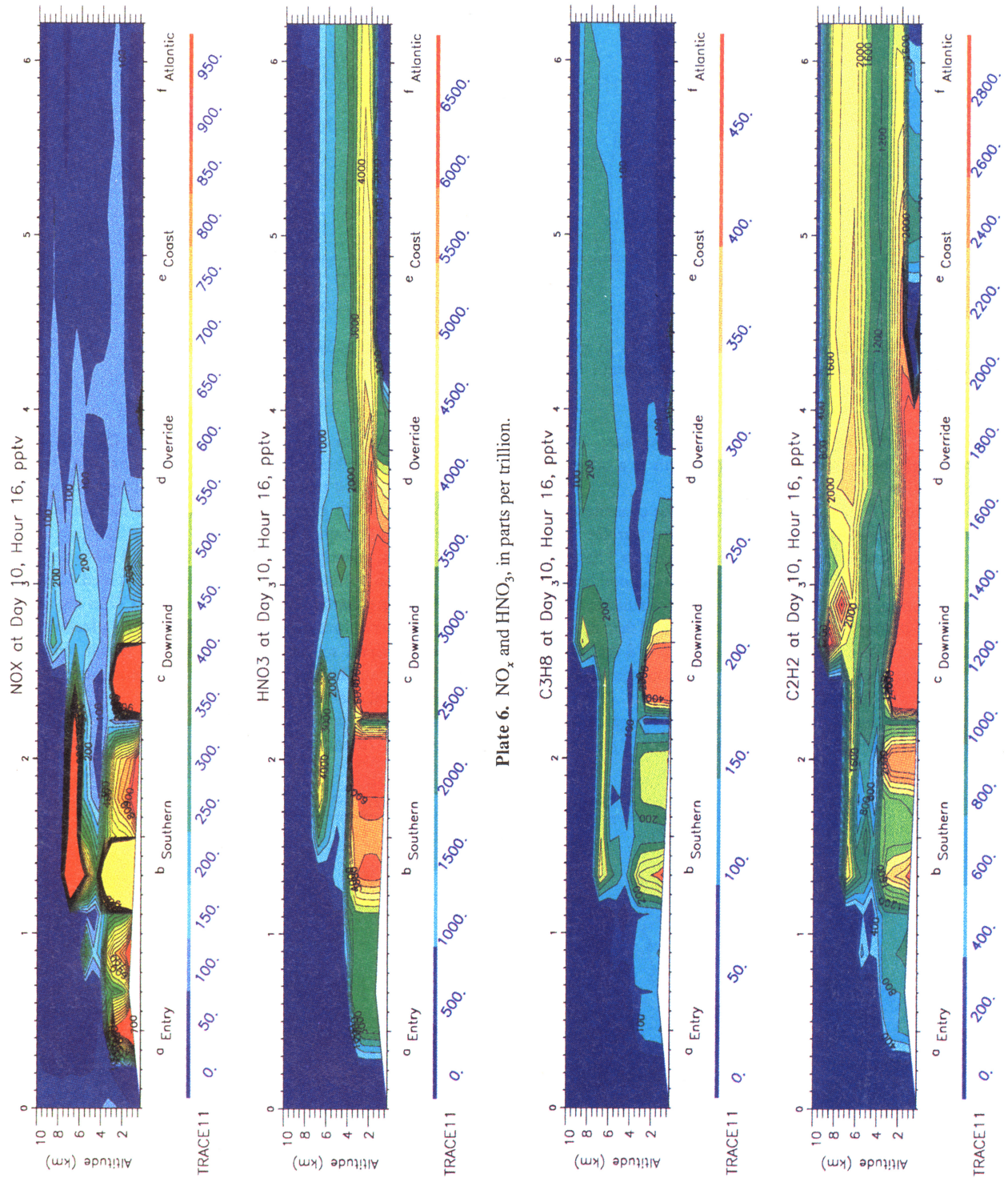


Plate 6. NO_x and HNO₃, in parts per trillion.

Plate 7. Acetylene and propane, in parts per trillion. Note that a portion of higher alkane emissions were lumped in with propane.

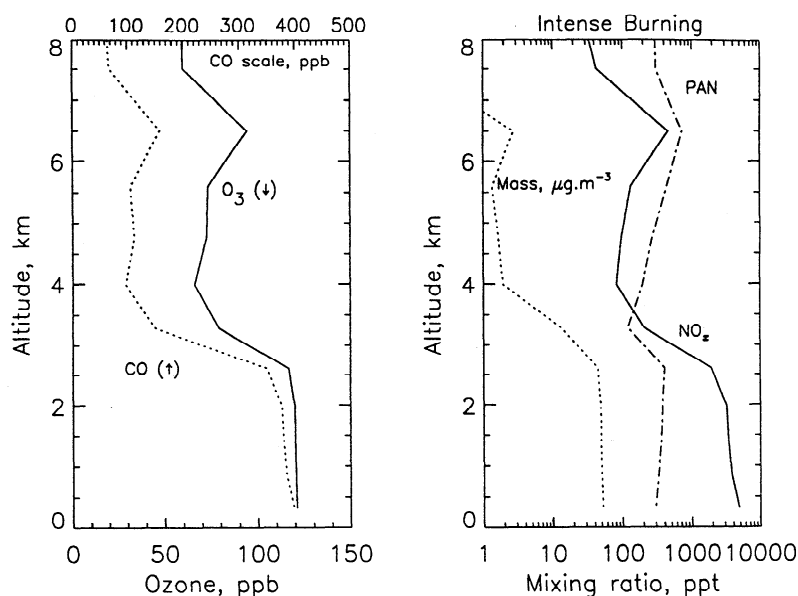


Figure 5a. Same compounds as Figure 4a in intense burning region at about 2400 km downwind, with both accumulated pollution and intense local burning.

concentrations and current removal efficiencies; better comparisons might be derived from the data. This is a subject to further investigation.

Upwind Region. The profile of several species concentrations in an upwind southern African plateau region (near the 1600 elapsed-kilometer mark of the contour plots, labeled "b") has been brought together into Figure 4a. CO, which acts as a good integral measure of pollution, reaches 130 ppb up to 3 km altitude (2 km over the surface) during the afternoon (1600 LT) and then drops to concentrations from 95–115 ppb in the region up to 8 km, with a spike to 150 ppb at 7 km. (CO in TRACE A was measured by the G. Sachse group of NASA Langley, (see *Collins et al.* [1995] for details.) Model profiles at 1000 LT (not shown) suggest lower concentrations in a shallower mixed layer. Figure 4b shows

measurements made on TRACE A flight 9 (1530 UT or ~ 1730 LT) near Johannesburg. Similarly, these exhibit lower tropospheric CO ~ 110 ppb, dropping to midtropospheric values of 85 at 5 km, but with general levels of 100 ppb and spikes of ~ 110 ppb at 7 km (compare to 150 ppb), while a 150 ppb spike appears at 10 km. Clearly, simulated and observed air have large variations as fresh pollution is being emitted and vented by cloud systems of varying depth. The 150 ppb spike of CO in the upper tropospheric observations may be better modeled as a feature of a plume from a distant source (see "character of ocean plumes," below). Firmer attribution would require a complete three-dimensional model analysis.

Ozone shows less variation in both simulation and observation, ranging from 65–75 ppb, comparing to 55–90, generally ~ 5 ppb

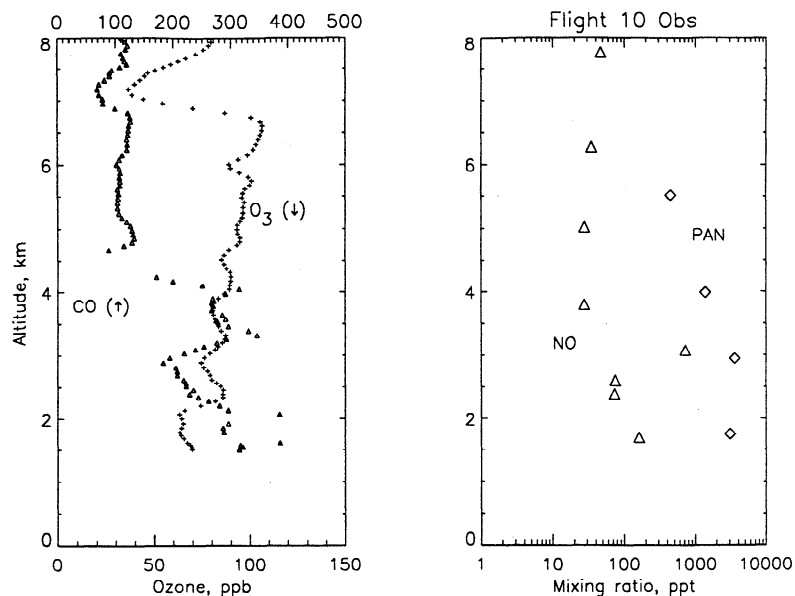


Figure 5b. An intense plume approximately 10°S and 29°E, near the south end of Lake Tanganyika sampled at close range by the NASA DC-8 in TRACE A.

higher, in the model (Figures 4a and 4b). Ozone data are taken from the TRACE A data archive, with technique described by *Browell et al.* [this issue]. A profile (not illustrated) simulated at 1000 LT is almost identical and compares well for CO also. Simulated PAN rises from 100 ppt to 600 ppt in the upper troposphere. There were few PAN measurements on this flight [*Singh et al.*, this issue] generally 500 ppt at 8 km. Flight 11, just east of the Indian Ocean, showed nonpolluted region concentrations of 100 ppt to 300 ppt. A substantial variation between morning (not shown) and afternoon in the simulations suggests, as do the contour plots, that this is a region of rapid pollution buildup. Observations would be expected to vary also, but there are relatively few comparison data from the DC-8 in this region. Actual atmospheric concentrations may also be affected by plumes with longer-range transport, as we suggested for the upper tropospheric 150 ppb feature above, possibly recirculating from southern or central Africa [*Tyson et al.*, 1995].

Source characterization region. Figure 7 shows the trace-species profiles well downwind in a region where many contour plots, Plates 4-7, have intense maxima. The region is 2400 km on the approximate elapsed-distance scale used there (just before "downwind"). The simulation, Figure 5a, shows a main plume extending up to 2 to 3 km, with a more dilute plume in the region 3.5-6 km; compared to regions above and below this is a lower region, though still polluted. Comparison to the *Collins et al.* [this issue] CO data, Figure 5b, is as good as might be expected.

A southern and central African "source characterization" flight (flight 10) showed an intense plume approximately 10°S and 29°E, near the south end of Lake Tanganyika. The air is our best sample of polluted central Africa, but is this air properly compared to "downwind" air and does this air get exported in the plume? The latter question is of concern for this paper and the investigations of marine plumes in the work of *Singh et al.* [this issue]. This sampling area is fairly far east in our sketched predominant travel pathway, and so the convergence and rising of pollutants may typically be fairly far north, if the meteorology of Plate 1, with its northeastward trending convergence line, can serve as a guide. If so, this air is also representative of source regions that influence plumes off the coast. (Three-dimensional analysis of this situation is no doubt rewarding but must be reserved for more study).

The sampling yielded CO values at 300 ppb and varying in the plume from 180 to 380 ppb between the surface upward 3 km to 4 km, at around 1020 UT or local noon; an intense emission source in the model at approximately -10° gives 300 ppb between 0 and 2 km at 1000 LT; Both the drop-off of CO and the vertical integrals of CO concentration in this polluted region are very similar to observations. Recall that the vertical spread in the model is determined by the mixed layers described in the three-dimensional model; however, the topography of the surface does not match the specific region sampled. Both simulated and observed ozone show a much deeper region of high values. The observations show an increase from 70 ppb near the surface to 100 ppb at 5.5 km. However, for this situation, simulated ozone drops with height, with values of 100 ppb to 75 at 4 km and back to 100 at 7 km. The UV DIAL ozone retrievals also suggest near-surface titrations, a preponderance of 90 ppb levels, with excursions to 100, i.e., somewhat better agreement than the in situ observations but increase not decrease, with altitude. Acetylene and especially propane [*Blake et al.*, this issue] are somewhat more enhanced in the simulation than CO; recall however, that simulated propane has some higher alkane emissions lumped in and allowing for this makes the correspondence better.

Observed NO (technique of *Smyth et al.* [this issue]) similarly decreases with altitude from above 200 ppt at 1.5 km to ~100 ppt, with a spike of 600 ppt at 3 km, reflecting nearby surface fire emissions. Simulated NO_x values show 2000 ppt at 1.5 km to values falling to 180 ppt values at 3.5 km, with no elevated pollution spike. (Only NO values, which are directly measured, are shown in Figure 5b. NO should mirror NO_x profiles with an overall factor of 0.25 to 0.3 dependent on time of day and ozone. For further discussion, see *Jacob et al.* [this issue].) Parts per billion of PAN were measured by *Singh et al.* [this issue], in the intense emission region (Figure 5b), but as the contour graphs suggest, no more than 300-400 ppt were typically simulated. We attribute these differences in part to the "quadratic pollutant concentration effect," though the simulation may have other problems also (missing some sources of peroxyacyl radicals). Natural nonmethane organics may add to the peroxy acetyl radical pool producing PAN, though as we indicated in the "chemical mechanism" section above, tree-derived isoprene did not seem to add very much to the burning-derived organic mix observed. In any case, the boundary layer PAN undersimulation and the NO_x overprediction may explain why this lower-tropospheric ozone is oversimulated, while CO is slightly undersimulated: too much NO_x is available in the model allowing excessive ozone production; however, this may be overinterpretation, and local modeling analysis is indicated, if feasible.

Some plumes are matched in the comparison of simulation to observation; some are simulated fairly at the right altitude and with appropriate concentrations. Since the cloud detrainment heights are chosen, detailed agreements are basically a matter of luck, or, of course, "tuning." Actual meteorology and emissions vary considerably from day to day. What the comparison illustrates is that the cloud detrainment idea can give the reproduce observations over 5 km, with CO plumes up high and CO ventilation (lower values) within the first few kilometers. The poorer match below 4 km suggests that boundary layer and cloud transport are complex, and it is more difficult to reproduce the vagaries of shallow clouds, topography, stable layers, and horizontal diffusion of plumes in a simple model. The broad features of "shallow" (3 km) NO_x and CO plumes and deep (8 km+) ozone plumes can be generally reproduced in a model with only clouds and the venting of biomass burning emissions. In other words, high NO_x (e.g., from lightning [*Smyth et al.*, this issue]) is not required in this situation to produce substantial ozone throughout the whole troposphere. Lightning NO may, of course, be quantitatively important in determining the ozone levels reached. Still, ozone freed from near-surface processes (NO reaction, deposition) effectively rises to disproportionately higher levels than its companion primary pollutant, CO. More analysis of this process may be found in the work of *Chatfield and Delany* [1990] and below.

The TRACE A data set on the emissions is necessarily limited, and does not give, region by region, a sufficient statistical background by which to judge our necessarily averaged model. We anticipate that better comparisons will be available as we are able to place in context the September SAFARI measurements reported by *Zenker et al.* [1995].

Modeled Ozone is Mostly "Cook and Mix"

Character of the oceanic ozone plumes. There tended to be offshore winds at the 3 - 6 km, often higher, in the region between 20°S and 3°N during the first half of October 1992, according to European Center. We have suggested that the Great African

Plume tends to the African coast in this region to affect the Atlantic Ocean in an equatorial flow, the "main path," or in an "alternative path" proceeding into a southern hemispheric anticyclone. The DC-8 aircraft sampled this area extensively on October 14 and 15, 1992, in "African outflow" flights. Analyzed winds and our three-dimensional simulation (under continuing analysis) suggest that the flow was changing from a southward "alternative pathway" during this period to a directly westward flow, the main path. Figure 6a and Figure 7 show versions of the outflow depicted in Figure 1. Figure 6a shows conditions 700 km offshore (5500 km elapsed distance), and Figure 7 conditions 1200 km offshore (marked "f Atlantic"): many features are very similar, suggesting that little net chemistry, i.e., ozone production, occurs in the simulation. We shall discuss ozone production below.

In the marine boundary layer, ozone diminishes between the more distant region of Figure 7 (upwind for the reverse-flowing marine boundary layer) and near-coast Figure 6. Input of ozone from above appears to be countered by low-NO_x ozone destruction. Singh *et al.* [this issue], Heikes *et al.* [1995], and Jacob *et al.* [this issue] have further discussion of this chemistry.

Plate 9 provides a south-to-north survey along 9°E made early in flight 13. The aerosol-controlled relative scattering signal provides a rich two-dimensional cross section of the Great African plume. It suggests that there was a main plume topping just over 4 km at the northern end, about 5°S. Figure 6b shows a profile of CO, O₃, NO, and PAN measured onboard the airplane at this northern edge; indeed, the right edge of Plate 9 is determined by the airplane path. The variations in the cross sections of aerosol scattering and ozone in Plate 9 show vividly the limitations of a

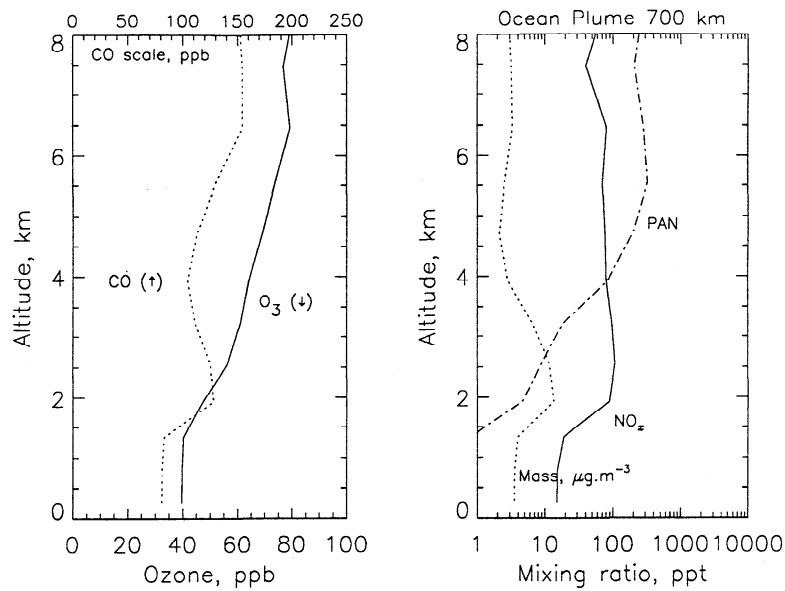


Figure 6a. Simulated near-coastal plume values for the same compounds as Figure 4a. Note the transition at 1.5 – 2 km, the top of the marine boundary layer. Compare with Figure 8.

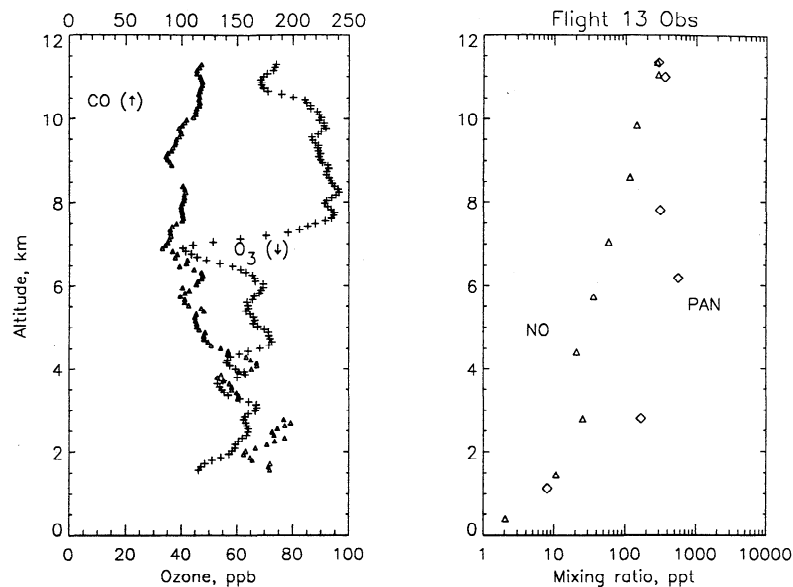


Figure 6b. Observations of an intense oceanic plume at 1020 UT near 6°S on flight 13.

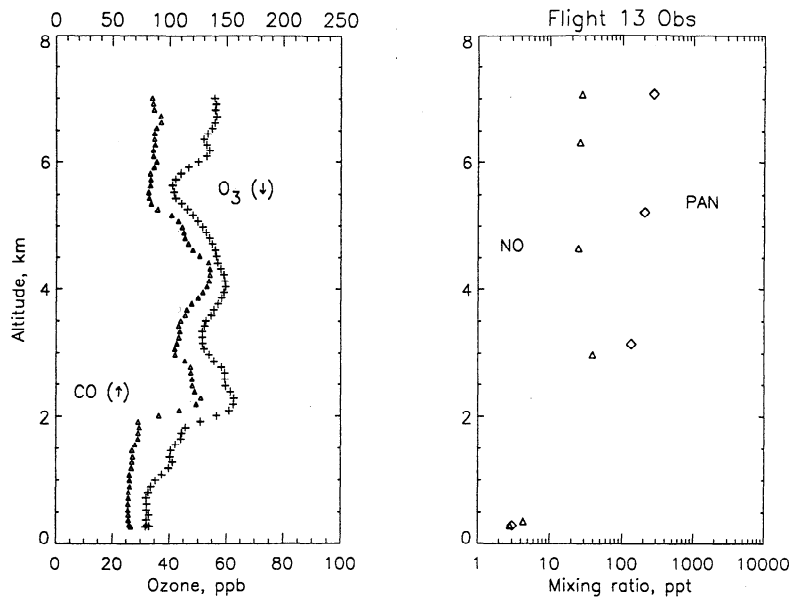


Figure 6c. Observations of a weaker plume near 18°S on flight 13 at 1230 UT.

two-dimensional model in this analysis: there are variations in the plume concentrations by factors of 5 within a degree latitude and even within a half kilometer in the vertical. Figure 6c shows another profile made farther south, at approximately 18°S, where the UV DIAL lidar data (not shown) suggest that the aerosol plume is much less intense.

The CO simulations of Figure 6 agree with the data generally in showing a plume reaching from 1.5 km to 3.5 km in the model, compared to 1.5 km to 4 km in Figure 6b (north) and 1.9 to 2.9 and 3.4 to 4.4 or 5 km in Figure 6c (south). Maximum CO concentrations are 130 ppb in the model, as compared to 165 in the Figure 6b peak and 130 and 140 in Figure 6c peaks. Our conceptual model (Figures 1 and 3) suggests that all of these

plumes are derived from shallow forced convection, predominantly boundary layer mixing, over the land. The variations in the plume top shown in Plate 9 would reflect the plume origins, not local conditions: the higher tops would have originated over hotter, drier, possibly higher, tropical land surfaces. We have assumed an anticyclonic-region subsidence in Figure 2 (see discussion in the work of *Singh et al.* [this issue] for values), which would not explain the higher plume top. This is the process keeping a sharp lower edge on the modeled plumes and, we expect, on the observed plumes. The upper plume should probably be simulated as more dilute; this could occur if detrainment extended to 12–14 km. Higher concentrations of CO have been noted in the upper troposphere, e.g., 160 ppb at the

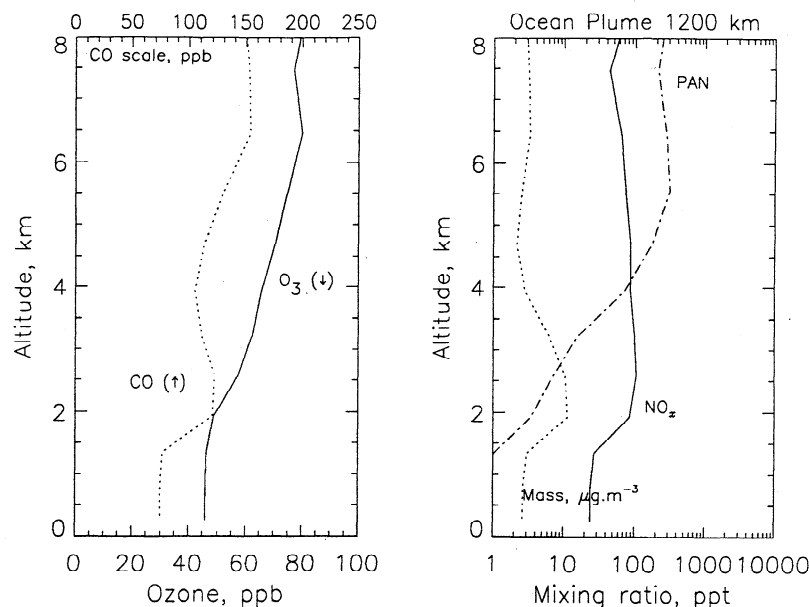


Figure 7. Further plume values for the same compounds. Notice very small changes in ozone and carbon monoxide. The latter is mostly influenced by gentle subsidence into the clean marine region below 1.0 km.

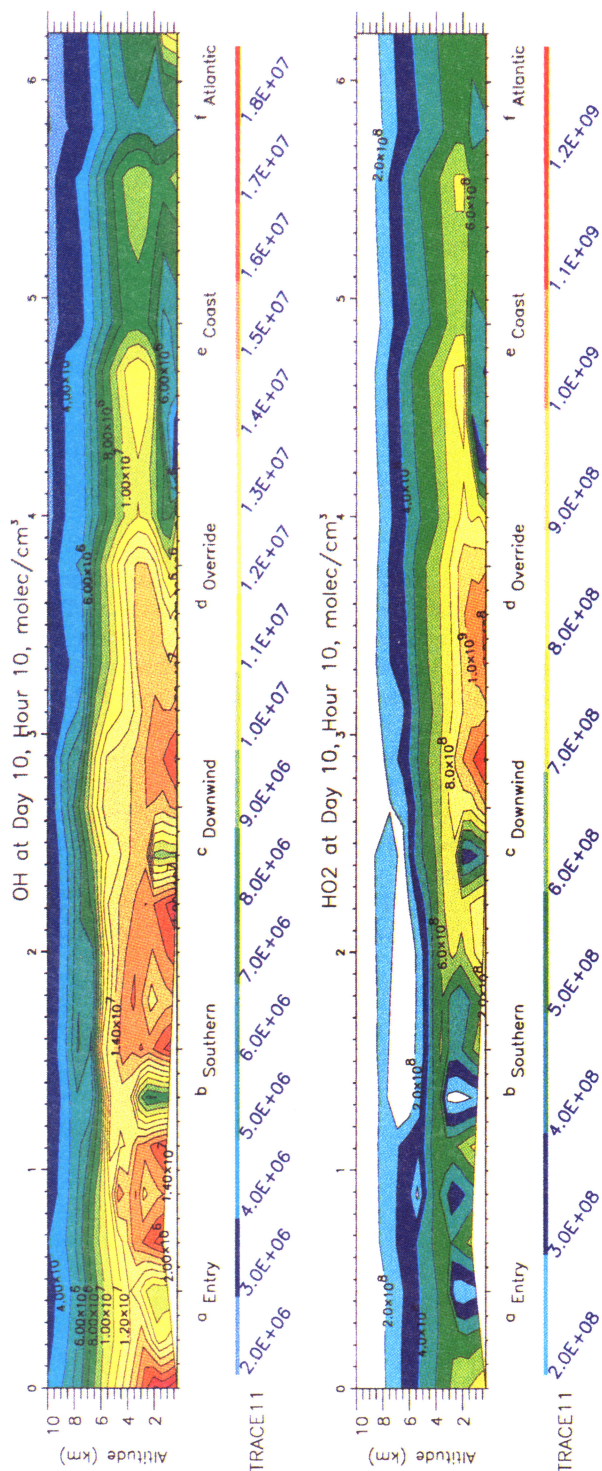


Plate 8. OH and HO₂ radical concentrations, in molecules cm⁻³; these species show the vestiges of previous days' emission patterns, as a sequence of small blobs on the oceanic plume.

beginning of flight 9, off the coast of Brazil. Restricted areas of even higher concentrations are also strongly suggested in our three-dimensional simulation.

High extent of the ozone continental plume. Both the simulations and the high-altitude observations of Figure 6b show an ozone plume continuing to rise as the CO plume drops in concentration. This region above 4 – 5.5 km is the cloud-transport-influenced region. As our discussion of the contour plots suggested, aerosol mass has “continental” plume lowest in vertical extent, carbon monoxide, transmitted by clouds, a partial midtropospheric presence, ozone a higher level, and PAN has an upper tropospheric plume only. The latter two have special chemistry favoring upper tropospheric plumes. These trends are seen in both the models and the observations of Figures 6 and 7 and Plate 9. Simulated ozone concentrations fall between the observations of Figures 6b and 6c. The 90 – 98 ppb maximum concentrations of Figure 6b surpass the upper tropospheric plume maxima of 80 – 85 ppb simulated for cloud-influenced maxima (Plate 4), but the general agreement seems satisfactory.

PAN also has a “high plume,” though it never reaches values over 300 – 500 ppt in the simulation seen at the 6-km region in the observations (Figures 6b and 6c) perhaps the upwind boundary conditions should be set higher. On the other hand, perhaps this is due to the model's coarse vertical resolution and the quadratic pollutant concentration effect. The greater-than-linear increase of PAN is clearly noticeable in unreported sensitivity runs where very concentrated pollutant emissions are simulated: concentration of the same emissions of pollution to a few spots over land, with convection nearby, leads to a PAN plume near observed levels.

Ozone production. Despite the general success of the model in explaining the difference between primary-pollutant plumes like CO and secondary-pollutant plumes like those of ozone, the simulation highlights some differences with other analyses of the TRACE A data, differences that may be related to significant gaps in our understanding of chemistry. There is little difference in the ozone profiles of Figure 7 and Plate 9; indeed, a glimpse at the contour plot of Plate 4 suggests that modeled ozone, like modeled CO, is essentially transported horizontally from source regions in the center of the model. There is no indication of net production of ozone in the plumes depicted. *Jacob et al.* [this issue] report calculations of similar ozone loss in the near-continental plume that we describe, based on diel-steady-state simulations which use but do not explain the concentrations of longer-lived species like NO, NO₂, and organics. The calculations depend importantly on the measured presence of active nitrogen oxides, NO_x, in the TRACE A data set. Our simulations have both ozone production and loss, but the net effect of production, loss, and a slow subsidence effect are to a slow, perhaps 0.5–1.0-ppb d⁻¹ decrease in ozone. *Jacob et al.* see production of ozone in the more distant upper troposphere, because of a process that does not seem to be consistent with our results: we do not describe any mechanism producing the required amount of NO_x. This is not a surprising feature of a model in which nitrogen oxides are largely bound into nitric acid, and PAN decomposition is too slow to resupply much more NO_x. The high levels of HNO₃ that we describe below reproduce some NO_x, but this production mechanism is probably not supported by the nitric acid data. That is, if our model got low values of HNO₃, we would have lower active nitrogen and more ozone destruction, less production than the observations suggest [*Jacob et al.*, this issue].

The behavior of ozone shown in Plate 4 may appear to represent a “mix and cook” depiction of the tropospheric ozone found in the equatorial Atlantic. This terminology was used by

AFRICAN OUTFLOW - WEST (DAY 1)
TRACE A FLIGHT 13 14 OCT 92

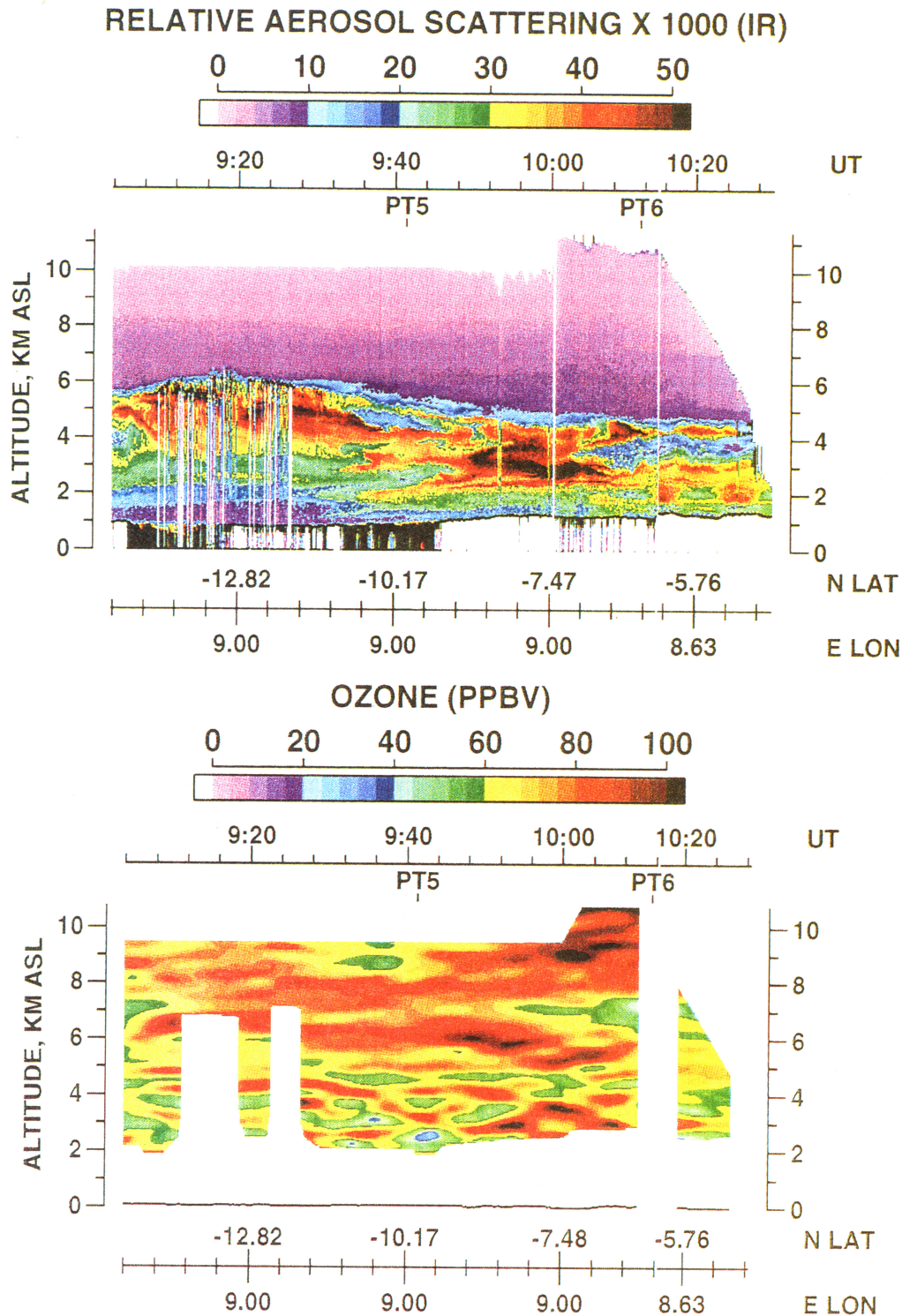


Plate 9. UV DIAL lidar returns from a survey of the Great African Plume off the coast of central Africa. The upper portion of the figure shows relative aerosol scattering, a quantity related to aerosol mass density in a complex way [Anderson *et al.*, this issue, and references]. The bottom portion of the plate shows ozone retrieved by differential absorption of the returned lidar signal. Both retrievals end at the top of the marine boundary layer, typically cloud covered. Note the discontinuity of the aerosol signal at 4.6 – 6 km altitude and the regions of especially concentrated smoke pollution. In contrast, note the smooth transitions of the ozone signal at this level. Compare to simulations, Figures 6 and 7 for aerosol and ozone.

Chatfield and Delany [1990], primarily to describe processes near continental convection. It refers to the lofting of fairly fresh emissions of NO_x so that some continued production of ozone may occur under high efficiency in the upper troposphere, but relatively near the cloud detrainment region, ~ 1 day's travel time downwind. Evidence of a predominant "cook and mix" process, in which ozone and its precursors have reacted rather fully and are then lifted in clouds, might indeed be seen in the region from "downwind" to "override" in Plate 4, for in that region there are features of approximately 5 ppb increase in ozone just downwind of convective towers. The "mix and cook" process is active in the deep continental boundary layers even in this simple model. Emissions and convection are also varying in time and, consequently, no further budgeting is attempted in this paper. However, all the ozone is essentially at the same levels as seen near the surface, and ozone increase extends for less than a day downwind (a couple of degrees).

A more extended interpretation of the "mix and cook" mechanism is that there is continued ozone increase far downwind in the Atlantic region depending somehow on the remote continental emissions but not accomplished over the continents. Some of the *Jacob et al.* [this issue] analyses for the more remote and higher-altitude Atlantic troposphere suggest a need for continued increase; most, the nearer, lower regions seem not to require continued production. An argument for continued net ozone production might be constructed from the portrayals of averaged tropospheric ozone residual [*Fishman et al.*, 1991; *Olson et al.*, this issue; *Thompson et al.*, this issue], which suggest a higher ozone column in the Atlantic than over Africa. However, this is only one interpretation of those results. *Smyth et al.* [this issue] suggest the possible role of lightning-generated nitrogen oxides; these would also have a land origin, but might be more broadly dispersed, coming from every thunderstorm, not just those venting pollutant NO_x. A possibility that *Jacob et al.* [this issue] mention is the possibility of re-NO_x-ification, as mentioned in a previous work of that group and by *Chatfield* [1994]. Those analyses suggest that there is much less HNO₃ in observations

than models suggest, and more NO_x, raising the possibility of NO_x return. Simple theory suggests HNO₃ / NO_x is near 20 in the midtroposphere.

This model repeats, in the context of the tropical ozone buildup, that current multidimensional models tend strongly to the "cook and mix" description of ozone buildup and that PAN or any other known nitrogen reservoirs do not contribute to sufficient transport of nitrogen oxides to explain the NO_x and possible ozone production observed. Computations made on the oceanic plume sections of Plate 6 suggest the nitric acid to NO_x ratio is high, ~ 20:1, even in the presence of some clouds and PAN. Failing continued NO_x production from a depleting reservoir like PAN, *Chatfield* [1994] argued the known meteorological and chemical data strongly imply these high ratios, so that a missing process, presumably condensed phase, needed investigation.

A near-surface nitric acid dilemma. An equally large disagreement between our simulation and observations is in the HNO₃, which is the major component of NO_y below 4.5 km throughout the model. Simulated HNO₃ reaches levels of 4 to over 10 ppb in the model (refer back to the plume contour plot, Plate 4), even though the concentration patterns clearly show the effect of dry deposition and removal in cloudy areas. Figure 8 shows profiles in the model extracted from the data defining the contour plot of Plate 4. It traces the buildup from an entry region, with concentrations dictated by the measured climatology [*Talbot et al.*, this issue] through initial and intense burning, and onward to two plume profiles. Predicted concentrations reach nearly 20 ppb downwind of the intense burning and fall back to several parts per billion. However, the HNO₃ values measured by *Talbot et al.* [this issue] reach only about 600 ppt. Some error in simulation of the order of 5 to 10 times is suggested. Any overprediction of nitric acid vapor in trajectory and other simple models can be attributed to their lack of realistic surface deposition processes and rainout. This simulation has both.

Why are the modeled levels so high in the presence of depositional and rainout? The same feature that explains lifting of pollution to the westward wind regions of the western African

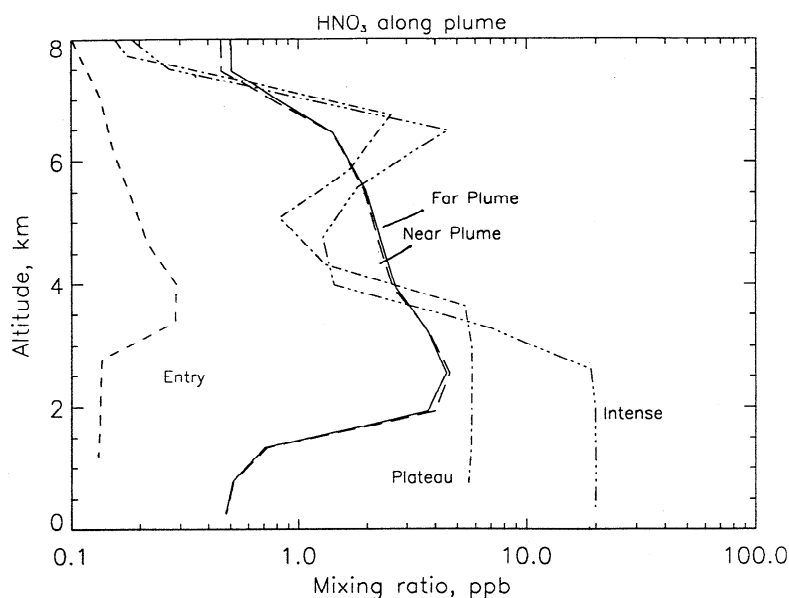


Figure 8. Simulated nitric acid profiles showing accumulation of nitrogen in this reservoir along the plume (parts per billion by volume) and occasional removal by venting and solution to rain. These values are very much higher than observations. Profiles are plotted at approximately the following positions along the top ("downwind distance") axis of Figure 2 and Plates 4-8. Entry, $0.9 \times 10^{+3}$ km downwind; plateau, 2.2; intense, 2.9; near plume, 6.0; and far plume, 6.5.

coast, the high planetary boundary layer heights reached in tropical dry regions, has also the effect of reducing dry deposition. The depositional timescale for a reactive gas is essentially the boundary layer height divided by the effective deposition velocity for the gas at the middle of the boundary layer. Essentially, this says, a molecule of HNO₃ gas has much more room and time to wander vertically before finding a ground surface to which to stick. The tropics allow much more dilution than in our midlatitude experience, where midday high boundary layers are frequently around 1000 m. All nitric acid taken into updrafts is removed; but below-cloud washout was not modeled, since it acts on much more limited volumes of air in a convective situation. The removal of nitric acid is shown in the decrease of HNO₃ from 10 (intense burning) to 3–4 ppb (in the plumes). Our simulation thus predicts that cleansing by cloud processes is also not sufficiently active to remove nitric acid either.

PAN provides one other check on our simulation. Despite its complex dependence on available organic reactants, it seems to be simulated reasonably well. That is, the observed concentrations show higher values than the simulation, rather than lower. This could be due to higher background PAN, or to the quadratic pollution concentration effect. The extra N sequestered in observed PAN cannot account for the HNO₃ shortfall. Further, the amount of NO_y emitted is consonant with the CO and organics emitted and therefore should be sampled, once the amounts taken out by ventilation and dry and wet deposition are accounted for. The emission on NO_x is largely constrained by the carbon emitted, to perhaps the 40% leeway we have taken in assuming a fuel nitrogen content (which we have argued may be accounted for anyway, via a soil nitrogen source).

For another check on our simulation, consider another species which is easily removed by precipitation. Figure 9 shows that hydrogen peroxide concentrations in the model are also quite high, reaching 2.8 ppb in the burning plume and not decreasing much downwind. However, these are very close to the 2.6 ppb levels reported for TRACE A [Singh *et al.*, this issue; Heikes *et al.*, this issue] and also show features of wet removal along the pathway.

Similarly, Plate 7 shows that smoke aerosol is observed far out into the Atlantic middle troposphere, rather than being strongly removed by clouds. Thus although Plate 1 may be construed to suggest that all air vented to the midtroposphere could go through a precipitating cloud region, removing nitric acid, hydrogen peroxide, and smoke patterns seem to deny this, as do the nitric acid concentrations observed in the “source characterization region.”

We simulated no heterogeneous process on aerosols for peroxide or nitrate. It is easy to imagine that a compound like H₂O₂ could react heterogeneously on aerosols and leave little trace. However, our comparison to data suggests that not much net reaction is required. Explaining the nitric acid poses a more severe problem, and it seems to be a somewhat different problem from the midtroposphere and uppertroposphere re-NO_x-ification problem [Chatfield, 1994]. While nitric acid may well have interactions with aerosol, the nitrogen residing there, or reemitted, should be found in some form, e.g., particulate nitrate, NO_x [Chatfield, 1994], or some organic nitrate. That is, it remains within the air mass until scavenged. No such nitrogen species was observable during the TRACE A mission, and our simulation predicts that cloud rainout and dry deposition are not likely to explain the absence of nitrogen: the processes are too slow. It is necessary to remove the nitrogen completely from the atmosphere, and we are now investigating the possible role of large particles, i.e., dust, smoke-generated or biogenic aerosols, which may settle or stick effectively to surfaces.

Conclusions

An idealized model describing the emission, transformation, and intercontinental transport of biomass burning and natural emissions from tropical countries seems to largely reproduce the general patterns of gaseous and aerosol trace species, as observed in TRACE A. The model incorporates land/sea differences, topography, and their influences, such as the overriding of hot, dry continental air above cooler forest and oceanic layers. It simulates

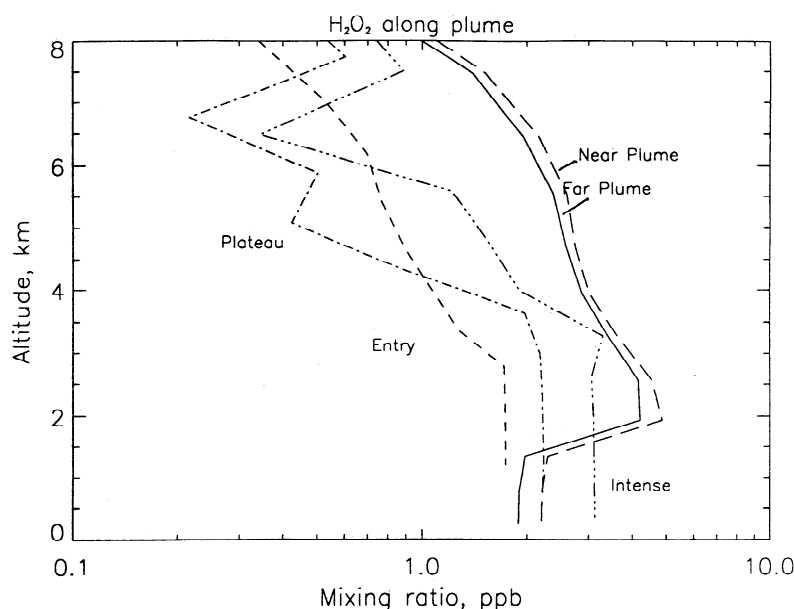


Figure 9. Simulated hydrogen peroxide profiles showing accumulation of H₂O₂ and its wet removal. Plume values (between 0 and 4 km altitude) are similar to observations, suggesting that wet removal processes are acting appropriately in the model (see text). Profile locations as in Figure 8.

deep cumulus convection, with raining updrafts and downdrafts. Shallow fair weather convection is ignored, being treated as a phenomenon of the planetary boundary layer. It is strongly guided by simulations made with three-dimensional assimilation runs, using MM5. While we must emphasize that CO was used to estimate the spatial pattern of clouds for the model, comparisons with results illustrate some virtues in the simulation in that (1) it can fit the CO (that is, deep boundary layers and clouds can explain the vertical transport where trajectories and eddy diffusion theory cannot) and that (2) the mass fluxes and cloud locations are in appropriate agreement with three-dimensional model results.

Though the pattern we idealize is not constant or persistent, three-dimensional work in progress suggests that it is common. Moreover, when it does recur, it tends to fill the equatorial Atlantic with a new burden of pollution. That burden is free to meander slowly westward in the equatorial winds, forming the Great African Plume or to be incorporated in anticyclones, especially the common anticyclone over southern Africa, following an alternate path.

The implementation of these details allows the model to distinguish a wide variety of chemical signatures that have commonly been described as biomass burning plumes. The CO pattern is the most general description of the Great African Plume, since CO is almost unreactive on this timescale. It fills the troposphere, though with strongest impact in the lower atmosphere. The aerosol signature, commonly defined as "the" biomass burning plume, is an essentially lower-tropospheric phenomenon which is well simulated as very strongly determined by removal of most aerosol mass in cloud updrafts of any significant depth. Ozone and especially PAN plumes are much more upper tropospheric phenomena.

The concentration profiles we show are in generally good agreement with TRACE A observations made from the DC-8. There are many separate features, with a variety of species, to match over a wide vertical and horizontal range. When emissions and ventilation are chosen to represent the vertical distribution of a tracer like carbon monoxide, the transport and wet removal of other species like ozone and hydrogen peroxide also tend to fall into agreement.

This agreement may help assure us that high-emission strengths of pollutants, such as are suggested by the Hao and Liu estimates, are reasonable, although they require systematic checking with more direct observation [Kendall *et al.*, 1995]. More work is required to check in detail the agreement of the idealized model with the three-dimensional simulations (e.g., Plate 2) and observations, though a factor of >2 discrepancy (see the Kendall, 1995) appears unlikely. Several points must be admitted, however. Lower-emission strengths of CO and NO_x may agree with a model with less ventilation, i.e., especially lower horizontal effective winds. (Altering cloud transport mass fluxes produces unacceptable CO profiles.) Other emission sources, e.g., biogenic sources of CO and NO_x, may also explain the distributions found in the atmosphere. This point is most salient for the nitrogen emissions, for we were forced to use assumed fuel nitrogen perhaps 40% higher than generally used for averages, although within the observed range. Lower emissions did not make enough ozone throughout the model domain. Other nitrogen sources, near the surface (G. Harris, unpublished data, this issue) or aloft [Jacob *et al.*, this issue; Chatfield, 1995] may help provide this active NO_x.

In short, we found fairly good representation of CO and aerosol distributions. Ozone was simulated fairly well: a vertical gradient increasing ozone in the upper troposphere appeared, but middle

and upper tropospheric O₃ levels were a bit below the observed values, indicating a possible need for more production in the upper troposphere. This would fit also with an midtropospheric source of NO_x.

Most comparisons of our idealized model to observations gave expectable agreement; the nitrogen comparisons did not. Since our simulation, with wet and dry deposition of nitric acid included, did not remove sufficient nitrogen from the atmosphere, we are forced to consider the possible role of large particles from smoke or biogenic sources.

A variety of meteorological phenomena were included in our simulation, a raised scarp where emissions were at several kilometers, a deep boundary layer mixing, and cloud transports. We found that the deep boundary layers, timed to maximize when emissions were highest, were instrumental in feeding polluted air from southern Africa to the near-equatorial region. Here the Great African Plume became particularly noticeable at 2–4 km altitude; topography played a smaller role. At least in this two-dimensional study, air could flow back down to lower altitudes without leaving remnant plumes at high altitude. Cloud convection was also relatively important in allowing CO and especially ozone and PAN to form elevated plumes. These were burning plumes that were essentially invisible because they had been cleared of smoke while going through precipitating clouds. They are, however, an equally significant intercontinental effect of biomass burning.

Acknowledgments. This research owes to the vision and support of Jack Kaye under NASA Research Program 579-24-13-10. Robert Chatfield particularly thanks Daniel Jacob and Anne Thompson for comments on this work. Andrew Ackerman, Christine Hlavka, and Hanwant Singh, all of NASA Ames, gave helpful advice and comments on this manuscript. An anonymous reviewer gave a thorough and appreciated critique. Many members of the TRACE A team contributed data and written analysis before publication. Paul Crutzen suggested interactions of N with smoke aerosol. Techniques of graphical visualization were developed in cooperation with the Environmental Protection Agency under an interagency agreement, DW80936544-01, and with the assistance of Robert Esswein; no EPA review or approval of the scientific content is implied.

References

- Anderson, B.E., W. B. Grant, G. L. Gregory, B. V. Browell, J. E. Collins Jr., G. W. Sachse, D. R. Bagwell, C. H. Hudgins, and N. J. Blake, Aerosols from biomass burning over the South Atlantic region: Distributions and impacts, *J. Geophys. Res.*, this issue.
- Andreae, M.O., et al., Biomass burning in the global environment: First results from the IGAC/BIBEX field campaign STARE/TRACE A/SAFARI-92, in *Global Atmospheric Biospheric Chemistry*, First IGAC Scientific Conference, Plenum, New York, pp. 83-101, 1994.
- Atkinson, R., Gas-phase tropospheric chemistry of organic compounds, *J. Phys. Chem. Ref. Data Monogr.*, 2, 1–216, 1994.
- Atkinson, R., et al., Evaluated kinetic and photochemical data for atmospheric chemistry: Supplement 1V, *Atmos. Environ.*, 25A, 1991.
- Bachmeier, A.S., and H.E. Fuelberg, A meteorological overview of the TRACE A period, *J. Geophys. Res.*, this issue.
- Blake, N.J., D.R. Blake, B.C. Sive, T.-Y. Chen, F.S. Rowland, J.E. Collins Jr., G.W. Sachse, and B.E. Anderson, Biomass burning emissions and vertical distribution of atmospheric methyl halides and other reduced carbon gases in the South Atlantic region, *J. Geophys. Res.*, this issue.
- Brenan, K.E., S.L. Campbell, and L.R. Petzold, *Numerical Solution of Initial-Value Problems in Differential-Algebraic Equations*, pp. 1-187, North-Holland, New York, 1989.
- Browell, E.V., et al., Ozone and aerosol distributions and air mass characteristics observed over the South Atlantic basin during the burning season, *J. Geophys. Res.*, this issue.
- Cahoon, D.R., Jr., B.J. Stocks, J.S. Levine, W.R. Coffey III, and K.P. O'Neill, Seasonal distribution of African savanna fires, *Nature*, 359, 812-815, 1992.

- Chatfield, R.B., Anomalous HNO₃/NO_x ratio of remote tropospheric air: Conversion of nitric acid to formic acid and NO_x?, *Geophys. Res. Lett.*, **21**, 2705-2708, 1994.
- Chatfield, R.B., and P.J. Crutzen, Are there interactions of iodine and sulfur species in marine air photochemistry?, *J. Geophys. Res.*, **95**, 22,319-22,341, 1990.
- Chatfield, R.B., and A.C. Delany, Convection links biomass burning to increased tropical ozone: However, models will tend to overpredict O₃, *J. Geophys. Res.*, **95**, 18,473-18,488, 1990.
- Collins, J.E., B.E. Anderson, G.W. Sachse, J.D.W. Barrick, L.O. Wade, L.G. Burney, and G.F. Hill, Atmospheric fine structure during GTE TRACE A: Relationships among ozone, carbon monoxide, and water vapor, *J. Geophys. Res.*, this issue.
- Connors, V.S., et al., Savanna burning and convective mixing in southern Africa: Implications for CO emissions and transport, in *Global Biomass Burning*, edited by J.S. Levine, pp. 147-155, MIT Press, Cambridge, Mass., 1991.
- Crutzen, P.J., A.C. Delany, J. Greenberg, P. Haagenson, L. Heidt, R. Lueb, W. Pollock, W. Seiler, A.F. Wartburg, and P. Zimmerman, Tropospheric chemical composition measurements in Brazil during the dry season, *J. Atmos. Chem.*, **2**, 233-2256, 1985.
- Crutzen, P.J., and M.O. Andreae, Biomass burning in the tropics: Impact on atmospheric chemistry and biogeochemical cycles, *Science*, **250**, 1669-1678, 1990.
- DeMore, W.B., S.P. Sander, D.M. Golden, R.F. Hampson, M.J. Kurylo, C.J. Howard, A.R. Ravishankara, C.E. Kolb, and M.J. Molina, Chemical kinetics and photochemical data for use in stratospheric modeling, in *Evaluation 11*, JPL Publ. 94-26, Jet Propul. Lab. Pasadena, Calif., 1992.
- Fan, S.-M., D.J. Jacob, D.L. Mauzerall, J.D. Bradshaw, S.T. Sandholm, D.R. Blake, H.B. Singh, R.W. Talbot, G.L. Gregory, G.W. Sachse, Origin of tropospheric NO_x over subarctic eastern Canada in summer, *J. Geophys. Res.*, **99**, 16,867-16,877, 1994.
- Fishman, J., Probing planetary pollution from space, *Environ. Sci. Technol.*, **25**, 613-620, 1991.
- Fishman, J., F.M. Vukovich, D.R. Cahoon, and M.C. Shipham, The characterization of an air pollution episode using satellite total ozone measurements, *J. Clim. Appl. Meteorol.*, **26**, 1638-54, 1987.
- Fishman, J., K. Fakhruzzaman, B. Cros, and D. Nganga, Identification of widespread pollution in the Southern Hemisphere deduced from satellite analyses, *Science*, **252**, 1693-1696, 1991.
- Fishman, J., J.M. Hoell Jr., R.D. Bendura, V.W.J.H. Kirchhoff, and R.J. McNeal, NASA GTE TRACE A Experiment (September-October 1992): Overview, *J. Geophys. Res.*, this issue.
- Fuelberg, H.E., J.D. VanAusdall, E.V. Browell, and S.P. Longmore, Meteorological conditions associated with vertical distributions of aerosols off the west coast of Africa, *J. Geophys. Res.*, this issue.
- Flossmann, A.I., and H.R. Pruppacher, A theoretical study of the wet removal of atmospheric pollutants, III, The uptake, redistribution, and deposition of (NH₄)₂SO₄ particles by a convective cloud using a two-dimensional cloud dynamics model, *J. Atmos. Sci.*, **45**, (13), 1857-1871, 1988.
- Garstang, M., P.D. Tyson, E. Browell, and R. Swap, Large scale transport of biogenic and biomass burning products, in *Biomass Burning and Global Change*, edited by J. S. Levine, MIT Press, Cambridge, Mass., this issue.
- Grell, G.A., Prognostic evaluation of assumptions used by cumulus parameterizations, *Mon. Weather Rev.*, **121**, 764-787, 1993.
- Grell, G., J. Dudhia, and D. Stauffer, A description of the fifth-generation Penn State/NCAR mesoscale model (MM5), *NCAR/TN-398+STR*, Natl. Cent. for Atmos. Res., Boulder, Colo., 1994.
- Hao, W.M., and M.H. Liu, Spatial and temporal distribution of tropical biomass burning, *Global Biogeochem. Cycles*, **8**, 495-503, 1994.
- Harris, G.W., F.G. Wienhold, and T. Zenker, Airborne observations of strong biogenic NO_x emissions from the Namibian savanna at the end of the dry season, *J. Geophys. Res.*, this issue.
- Heidt, L.E., J.P. Krasnec, R.A. Lueb, W.H. Pollock, B.E. Henry, and P.J. Crutzen, Carbon Monoxide, *J. Geophys. Res.*, **85**, 7329-7336, 1980.
- Heikes, B., M. Lee, D. Jacob, R. Talbot, J. Bradshaw, H. Singh, D. Blake, B. Anderson, H. Fuelberg, and A. M. Thompson, Ozone, hydroperoxides, oxides of nitrogen, and hydrocarbon budgets in the marine boundary layer over the South Atlantic, *J. Geophys. Res.*, this issue.
- Jacob, D. J., et al., Origin of ozone and NO_x in the troposphere: A photochemical analysis of aircraft observations over the South Atlantic basin, *J. Geophys. Res.*, this issue.
- Justice, C.O., J.D. Kendall, P.R. Dowry, and R.J. Scholes, Satellite remote sensing of fires during the Safari campaign using NOAA AVHRR data, *J. Geophys. Res.*, this issue.
- Kaimal J.C., J.C. Wyngaard, D.A. Haugen, O.R. Coté, Y. Izumi, S.J. Caughey, and C.J. Readings, Turbulence structure in the convective boundary layer, *J. Atmos. Sci.*, **33**, 2152-2169, 1976.
- Kauffman, J.B., R.L. Sanford Jr., D.L. Cummings, H. Salcedo, and E. V. S. B. Sampaio, Biomass and nutrient dynamics associated with slash fires in neotropical dry forests, *Ecology*, **74**, 140-151, 1993.
- Kendall, J.D., C.O. Justice, P.R. Downey, C.D. Elvidge, and J.G. Goldammer, Remote sensing of fires in southern Africa during the SAFARI 1992 campaign, in *Fire in the Southern African Savanna: Ecological and Environmental Perspectives*, B. van Wilgen, M.O. Andreae, J. G. Goldammer, and J.A. Lindsay, Editor, 1995, Witwatersrand University Press, Johannesburg, South Africa, 1995.
- Krishnamurti, T.N., M.C. Sinha, M. Kanamitsu, D. Oosterhof, H. Fuelberg, R. Chatfield, D.J. Jacob, and J. Logan, Passive tracer transports relevant to the TRACE A experiment, *J. Geophys. Res.*, this issue.
- Langaas, S., Diurnal cycles in savanna fires, *Nature*, **363**, 120, 1993.
- Lober, J.M., D.H. Scharfe, W.-M. Hao, T.A. Kuhlbasch, R. Seuwen, P. Wameck, and P.J. Crutzen, Experimental evaluation of biomass burning emissions: Nitrogen and carbon containing compounds, in *Global Biomass Burning*, edited by J.S. Levine, pp. 289-204, MIT Press, Cambridge, Mass., 1991.
- Logan, J. A., and V. W. J. H. Kirchhoff, Seasonal variations of tropospheric ozone at Natal, Brazil, *J. Geophys. Res.*, **91**, 7875-7881, 1986.
- Loring, R.O., Jr., H.E. Fuelberg, J. Fishman, and E.V. Browell, Influence of a middle-latitude cyclone on tropospheric ozone distributions during a period of TRACE A, *J. Geophys. Res.*, this issue.
- Lurmann, F.W., and A.C. Lloyd, A chemical mechanism for use in long-range transport/acid-deposition computer modeling, *J. Geophys. Res.*, **91**, 10,905-10,936, 1986.
- Madronich, S., and J. Calvert, Permutation reactions of organic peroxy radicals in the troposphere, *J. Geophys. Res.*, **95**, 5697-5715, 1990.
- Marengo, A., J.C. Medale, and S. Prieur, Study of tropospheric ozone in the tropical belt (Africa, America) from STRATOZ and TROPOZ campaigns, *Atmos. Environ.*, **24**(A), 2823-2834, 1990.
- Nganga, D., A. Minga, B. Cros, C. Bouka Biona, J. Fishman, and W.B. Grant, The vertical distribution of ozone measured at Brazzaville, Congo, during TRACE A, *J. Geophys. Res.*, this issue.
- Olson, J.R., et al., Results from the IPCC Photochemical Model Intercomparison (PhotoComp): Some Insights into tropospheric chemistry, *J. Geophys. Res.*, 1996.
- Olson, J. R., J. Fishman, and V. W. J. H. Kirchhoff, An analysis of the distribution of ozone over the southern Atlantic Ocean, *J. Geophys. Res.*, this issue.
- Patterson, E.M., C.S. Kiang, A.C. Delany, A.F. Wartburg, A.C.D. Leslie, and B.J. Huebert, Global measurements of aerosol in remote continental and marine regions: Concentrations, size distributions, and optical properties, *J. Geophys. Res.*, **85**, 7361-7376, 1980.
- Pickering, K. E., et al., Convective transport of biomass burning emissions over Brazil during TRACE A, *J. Geophys. Res.*, this issue (a).
- Pickering, K. E., A. M. Thompson, D. P. McNamara, M. R. Schoeberl, H. E. Fuelberg, R. O. Loring Jr., M. V. Watson, K. Fakhruzzaman, and A. S. Bachmeier, TRACE A trajectory intercomparison, 1, Effects of different input analyses, *J. Geophys. Res.*, this issue (b).
- Potter, C.S., P.A. Matson, P.M. Vitousek, and E.A. Davidson, Process modeling of controls on nitrogen trace gas emissions, from soils worldwide, *J. Geophys. Res.*, **101**, 1361-1377, 1996.
- Reichle, H.G., Jr., V.S. Connors, J.A. Holland, R.T. Sherrill, H.A. Wallio, J.C. Casas, E.P. Condon, B.B. Gormsen, and W. Seiler, The distribution of middle tropospheric carbon monoxide during early October 1984, *J. Geophys. Res.*, **95**, 9845-9856, 1990.
- Rew, R.K., and G.P. Davis, NetCDF: An interface for scientific data access, in *Computer Graphics and Applications*, pp. 76-82, Inst. of Electr. and Electron. Eng., New York, 1990.
- Roberts, J.M., Reactive odd-nitrogen (NO_y) in the atmosphere, in *Composition, Chemistry, and Climate of the Atmosphere*, edited by H.B. Singh, pp. 176-215, Van Nostrand Reinhold, New York, 1995.
- Rodin, L.E., and N.I. Bazilevich, *Production and Mineral Cycling in Terrestrial Vegetation* (Eng. Transl.), edited by G.E. Fogg, Oliver and Boyd, Edinburgh, 1967.
- Routhier, F., R. Dennett, D.D. Davis, A. Wartburg, P. Haagenson, and A.C. Delany, Free tropospheric and boundary layer measurements of

- ozone over the latitudinal range of 58°S to 70°N, *J. Geophys. Res.*, **85**, 7307-7321, 1980.
- Scala, J.R., M. Garstang, T. Wei-Kuo, K.E. Pickering, A.M. Thompson, J. Simpson, V.W.J.H. Kirchhoff, E.V. Browell, and G. Sachse, Cloud draft structure and trace gas transport, *J. Geophys. Res.*, **95**, 17,015-17,030, 1990.
- Scholes, R.J., J.D. Kendall, and C.O. Justice, The Quantity of biomass burned in southern Africa, *J. Geophys. Res.*, this issue.
- Seiler, W., The cycle of atmospheric CO, *Tellus*, **26**, 117-135, 1974.
- Seinfeld, J., *Atmospheric Chemistry and Physics of Air Pollution*, chaps. 12 and 16, John Wiley, New York, 1986.
- Singh, H.B., Impact of biomass burning emissions on the composition of the South Atlantic troposphere: Reactive nitrogen and ozone, *J. Geophys. Res.*, this issue.
- Smolarkiewicz, P.K., A fully multidimensional positive advection scheme with small implicit diffusion, *J. Comput. Phys.*, **54**, 325-362, 1984.
- Smyth, S., et al., Factors influencing the upper free tropospheric distribution of reactive nitrogen over the South Atlantic during the TRACE A experiment, *J. Geophys. Res.*, this issue.
- Talbot, R.W., et al., Chemical characteristics of continental outflow over the tropical South Atlantic Ocean from Brazil and Africa, *J. Geophys. Res.*, this issue.
- Thompson, A.M., K.E. Pickering, D.P. McNamara, M.R. Schoeberl, R.D. Hudson, J.-H. Kim, E.V. Browell, V.W.J.H. Kirchhoff, and D. Nganga, Where did tropospheric ozone over southern Africa and the tropical Atlantic come from in October 1992? Insights from TOMS, GTE TRACE A and SAFARI 1992, *J. Geophys. Res.*, this issue.
- Toon, O.B., R.P. Turco, D. Westphal, R. Malone, and M.S. Liu, A multidimensional model for aerosols: Description of computational analogs, *J. Atmos. Sci.*, **45**, 2123-43, 1988.
- Tyson, P.D., M. Garstang, R.J. Swap, E.V. Browell, R.D. Diab, and A.M. Thompson, Transport and vertical structure of ozone and aerosol distributions over southern Africa, in *Biomass Burning and Global Change*, edited by J.S. Levine, MIT Press, Cambridge, Mass., 1995.
- Wang Y., W.-K. Tao, K.E. Pickering, A.M. Thompson, J.S. Kain, R.F. Adler, J. Simpson, P.R. Kechn, and G.S. Lai, Mesoscale model (MM5) simulations of TRACE A and PRESTORM convective systems and associated tracer transport, *J. Geophys. Res.*, this issue.
- Zenker, T., et al., Regional trace gas distribution and air mass characteristics in the haze layer over southern Africa during the biomass burning season (Sep./Oct., 92): Observations and modeling from the STARE/SAFARI'92 /DC3, in *Biomass Burning and Global Change*, edited by J.S. Levine, MIT Press, Cambridge, Mass., 1995.

R. B. Chatfield and H. B. Singh, NASA Ames Research Center, MS 245-5, Moffett Field, CA 94035-1000.

G. Sachse, NASA Langley Research Center, Hampton, VA 23665-5225.

J. A. Vastano, Research Foundation, San Jose State University, San Jose, CA 95192.

(Received November 10, 1995; revised April 1, 1996; accepted May 30, 1996.)